ON THE USE OF DYNAMIC MODELS FOR STUDYING LAUNCH VEHICLE BUFFET

AND GROUND-WIND LOADS

By Perry W. Hanson and George W. Jones, Jr.

NASA Langley Research Center
Langley Station, Hampton, Va.

Presented at the Symposium on Aeroelastic
and Dynamic Modeling Technology

Dayton, Ohio
September 23-25, 1963

LIST OF ILLUSTRATIONS

SYMBOLS

$\hat{C}_L(k)$ correlation function

C_A aerodynamic damping coefficient

C_c control-system damping

C_{cr} critical value of damping

C_s structural damping coefficient

D reference diameter

f natural frequency

k reduced frequency, $L\omega/V$

L total length

ℓ reference length, usually diameter

l effective moment arm

M Mach number

M'_n generalized mass of nth mode

q dynamic pressure, $\frac{1}{2}\rho V^2$, $\frac{1}{2}\rho_e^2$

R_N Reynolds number

R reference radius

U_e equivalent ground-wind velocity

u random velocity fluctuations of ground wind in drag direction

v random velocity fluctuations of ground wind in lift direction

V free-stream velocity

Z_o any particular longitudinal station

σ^2 mean-square bending moment

σ root-mean-square bending moment

σ_T total root-mean-square bending moment, $\sqrt{\sigma_1^2 + \sigma_2^2 + \sigma_3^2}$

4

ϵ surface roughness height

ω circular frequency

ρ fluid density

PSD   power spectral density

Subscripts:

F   full scale

M   model

n   nth natural free-free bending mode, $\ n = 1, 2, 3, \ldots$

ON THE USE OF DYNAMIC MODELS FOR STUDYING LAUNCH VEHICLE BUFFET

AND GROUND-WIND LOADS

By Perry W. Hanson and George W. Jones, Jr.

NASA Langley Research Center

Langley Station, Hampton, Va.

ABSTRACT

The complex nature of the random aerodynamic input forces associated with transonic buffet and ground winds leads to difficulty in analytical treatment of the response of launch vehicles to these important loading conditions. The application of aeroelastically scaled models in the wind tunnel as a mechanical analog of the mathamatically complex problem requiring solution is described. Scaling relationships involved in this approach are developed and some checks on their validity are presented. Model design and support techniques are discussed and some typical results given. Some problems arising from the increased size of launch vehicles are discussed.

ON THE USE OF DYNAMIC MODELS FOR STUDYING LAUNCH VEHICLE BUFFET

AND GROUND-WIND LOADS

By Perry W. Hanson and George W. Jones, Jr.

NASA Langley Research Center

INTRODUCTION

Aeroelastic models of proposed aircraft or components have, of course, long been used to prove the stability of the design and to establish flutter and buffet boundaries. In view of the contributions that aeroelastic and dynamic model testing have made in the field of aircraft design, it is only natural that consideration be given to using such models for evaluation of launch vehicle designs. The relative importance of the various loading conditions on launch vehicles may be different with respect to those on aircraft structures but the reliable prediction of the loads is as important as ever.

This paper is concerned with the prediction of gross loads due to the response of lightly damped systems to the effects of separated flow. Two such load conditions are loads induced by ground winds and loads due to transonic buffeting.

As shown in figure 1, ground winds can be responsible for a variety of loading conditions. A drag load is produced in the direction of airflow that may be fluctuating due to atmospheric turbulence, gusts, etc. Vortex shedding can induce fluctuating loads in the direction of and perpendicular to the wind direction that may very well dictate strength requirements over a large portion of the vehicle.

Soon after lift-off the vehicle may be subjected to transonic buffeting loads, that, if not properly accounted for, could cause failure. Different types of buffet flow produce fluctuating pressures which can have quite different characteristics. An illustration of the differences in the power spectral density of the fluctuating pressures for two buffet flow conditions is given in figure 2. Although the total energy in each of the two pressure power spectra is about the same, it is seen that the distribution of energy is quite different. Most of the energy for the shock-boundary-layer interaction type of flow is in the low-frequency band; however, the wake buffet spectrum is nearly "white" and extends into the high-frequency range. The shock-boundary-layer interaction type distribution would be of concern for the booster elastic bending modes, whereas the wake buffet would contain energy of concern for higher frequency modes such as panel response.

The complex nature of these random aerodynamic input forces associated with transonic buffet and ground winds leads to difficulty in analytical treatment of the response of launch vehicles to these important loading conditions. Consequently, an extensive wind-tunnel launch vehicle buffet and

L-3468

ground-winds loads study program has been undertaken at the Ames and Langley Research Centers.

Most of the buffet data reported to date have been concerned with the fluctuating pressure input part of the problem. (See refs. 1 and 2, for example.) In reference 3 fluctuating pressure data are presented for different size models of a large manned launch vehicle tested in air and in Freon-12. Although pressure data play a significant role in understanding the overall buffet characteristics of a particular configuration, application of these input data in the prediction of gross structural response is usually quite difficult. However, a relatively simple loads prediction technique can be applied which makes use of an aeroelastically scaled model in a wind tunnel as a mechanical analog of the mathematically complex problem requiring solution. That is, a suitable model in a suitable wind tunnel first generates the correct aerodynamic input forces and then performs the very difficult time and space integrations producing the desired response which can be measured readily. The application of this concept to the two problem areas, gross bending response due to transonic buffeting and ground-wind loads, will now be discussed. Model design considerations, including the support system and scale factors, and the data analysis methods applied to the two problems are somewhat dissimilar. For instance, the ground-winds model must be essentially cantilevered perpendicular to the flow direction, whereas the buffet model must be supported in as nearly a free-flight condition as practical. Also the relative importance of scale factors is different for the two models. The major aerodynamic scale parameter for the buffet model is Mach number but Reynolds number is the primary aerodynamic scale parameter for ground-winds models. Because of these differences, the two areas of concern may be more conveniently discussed separately. First, consider the dynamically scaled aeroelastic model approach applied to the problem of predicting vehicle gross bending loads due to transonic buffet.

PREDICTION OF TRANSONIC BUFFET LOADS

Design Considerations

A suitable model is, of course, a prime requirement. In addition to properly scaling the mass and stiffness distributions of the launch vehicle, the model must be supported in such a manner that it is essentially free to respond in its "free-free" bending modes. Model designs at Langley satisfying these requirements to varying degrees have progressed from relatively simple models and mounting systems to rather complex ones. Shown in figure 3 is a simple aeroelastic model the stiffness of which is determined by the thickness of the fiber-glass shell. Lead ballast was fixed to reinforcing rings along the model length to obtain the proper mass.

A more sophisticated model, a 2-percent aeroelastic model of the Saturn SA-1, is shown in figure 4. Here again the stiffness distribution is determined by the thickness and radius along the model of the fiber-glass shell. The skeleton reinforces the very thin scalloped section in the radial or "hoop" plane and serves as instrument and ballast mounts while contributing negligible bending stiffness. The sting incorporates an air-cooled electromagnetic shaker and a model restraining device. The model is supported on the

sting by leaf springs attached to the model at the first free-free mode points.

Results of recent investigations (ref. 4, for example) have indicated that vibration modes higher than the fundamental flexural mode may need to be simulated. The power spectrum of bending-moment response for a configuration tested is shown in figure 5, which indicates that the first two elastic modes are of equal importance in defining total response of this particular configuration. Note the low level of response in the low-frequency range associated with the support system. It has been found that supporting the model at the first free-free node points on springs that are soft relative to the model flexural stiffness provides a system that introduces negligible restraint even in the higher modes. Shown in figure 6 are some calculated free-free mode shapes and frequencies of a model recently tested compared with the mode shapes actually measured on the model mounted on the support system. The agreement is considered to be very good, and indicates that the free-free modes were not unduly influenced by the mounting system. In addition to supporting the model so that it experiences a minimum of restraint in its free-free vibration modes, other factors need to be considered. The rigid body effective pitch stiffness may be simulated but the sting-support system bending frequency must not be near the flexible mode frequencies. Another requirement for the model support system is that a means be provided for measuring the structural and aerodynamic damping of the model since these parameters enter into the scaling relationships necessary for extrapolating tunnel test data to full-scale conditions.

An example of such a support system that has been used recently is shown schematically in figure 7. The model was supported on a sting by means of a system of cables, pulleys, leaf springs, and torque rod springs. The leaf springs, attached to the model at the forward and rear node points of the first free-free mode, restrained the model in the drag and yaw directions. They contributed approximately 25 percent of the pitch stiffness required to simulate the full-scale pitch frequency. The model weight was supported by cables (also attached to the model at the first free-free node points) reeved over pulleys on the sting and routed out the rear of the model to a system of torque springs outside the test section. These torque springs provided the remaining 75 percent of the required pitch stiffness. Figure 8 is a photograph of the sting and shows the water-cooled electromagnetic shaker field coils which were built onto the sting. The moving coils of the shaker were attached directly to the inside of the model at the rear. The shaker was used to excite the model in its elastic vibration modes in order to determine the aerodynamic damping in each mode. Also shown are the pulleys used to guide the weight-supporting cables down the sting and the pneumatically operated "snubbers" which were used to restrain the model motion with respect to the sting whenever the need arose. Another requirement to be considered, of course, is the suitability of the tunnel in which the model is to be flown. The larger the model it can accommodate, the lesser will be the fabrication problem. The tremendous size and low stiffness levels of launch vehicles already dictate drastically reduced scale models with the accompanying difficulty in realizing the low scaled stiffness levels required and yet making them strong enough to withstand the loads imposed in wind-tunnel testing. Needless to say, the tunnel must have the capability of operating through the transonic speed range at reasonable levels of dynamic pressure, and the turbulence level must be sufficiently low so that the buffet response is not obscured by the response to turbulence.

Buffet Loads Scaling Relationships

Wind-tunnel buffet loads studies rely on the validity of certain scaling parameters for extrapolating the model results to full-scale conditions. The usefulness of these parameters has been reasonably well verified for the airplane wing buffet problem. Some experiments designed to provide further insight regarding the validity of their application to the launch vehicle buffet case have been conducted in reference 3. Some typical results are shown in figure 9. In this figure, the power spectra of fluctuating pressures acting on rigid models of a launch vehicle configuration are presented. The spectra in the upper part of the figure are, essentially, raw data measured on two models which differed in size by a factor of five and which were tested in air and Freon-12. Consider the upper portion of figure 7(a) which shows data for a 1.6-percent and an 8-percent model tested in Freon-12. The two models produced two spectra which form separate functions of frequency out to the limit of the instrumentation of about 600 cps. The spectra of the lower portion of the figure have been scaled to full-scale conditions by scaling relationships which involve ratios of the dynamic pressure, velocity, and body diameter. The scaling relationships used are, for the ordinate

$$(PSD)_F = (PSD)_M \left(\frac{q_F}{q_M}\right)^2 \left(\frac{D_F}{D_M}\right) \left(\frac{V_M}{V_F}\right)$$

and for the abscissa

$$f_F = f_M \left(\frac{D_M}{D_F}\right) \left(\frac{V_F}{V_M}\right)$$

It can be seen that the spectra of the lower part of the figure could reasonably well be represented by a single function indicating that, in this case, the scaling relationships seem to be applicable at least over a range of five to one. Figures 7(b) through 7(e) generally indicate the same conclusion. Figure 7(b) presents data from a transducer located at a position different from that of figure 7(a), and the data in figure 7(c) are for a different Mach number and much lower pressures. Figure 7(d) compares data from a model tested in Freon-12 and in air. Finally, figure 7(e) compares the data from a 1.6-percent model tested in Freon-12 and an 8-percent model tested in air. Results of this type encourage the belief that model buffet data can be extrapolated to full-scale conditions. Further results concerning buffet pressure scaling are contained in reference 5.

In order to predict the magnitude of full-scale buffet loads from tests on dynamically scaled aeroelastic models, it is necessary, of course, to determine the proper scaling relationships for such a system. A dynamic analysis of launch vehicle buffeting has been considered in some detail in reference 4. In the analysis, based on simple beam theory and the techniques of generalized harmonic analysis (which is treated in some length in ref. 6 and was first applied to the analysis of buffeting in ref. 7), the vehicle was assumed to be flying at constant altitude with a constant velocity. The only aerodynamic forces present in addition to the random component were damping forces proportional to the velocity of the bending vibrations of the system. No loss of generality results from neglecting the aerodynamic inertia and spring forces since such forces usually are small when compared with their

structural counterparts for a slender launch vehicle (see, for instance, refs. 8 and 9). Structurally, the vehicle was considered to be a linear multidegree-of-freedom system.

The final result obtained from this analysis for the total root-mean-square bending moment at some longitudinal station Z_O is

$$\sigma_T^2(Z_O) = \sum_{n=1}^{\infty} l_n^2 \left[\frac{\pi \omega_n}{4\left(\frac{C}{C_{cr}}\right)_n} \right] \frac{q^2}{V} R^2 L^3 \hat{C}_{L,n}(k_n) \tag{1}$$

(Although eq. (1) has been developed for mean-square bending moment, it should be pointed out that expressions similar to eq. (1) could be obtained for any quantity which is proportional to displacement.) The total mean-square bending moment is a superposition of single-degree-of-freedom results (coupling terms were neglected in the derivation), each mode being independently treated as a separate system. The right-hand side of equation (1) may be conveniently separated into three parts. The first part, the term l_n^2, is the square of an effective moment arm. The second term, enclosed in brackets, is an admittance type term. In particular, it is $\pi/2$ times the maximum value of the mechanical admittance in the nth mode multipled by the width of the admittance curve at the one-half power point. The damping ratio which appears in the second term of the right-hand side of equation (1) is

$$\left(\frac{C}{C_{cr}} \right)_n = \frac{C_s}{C_{cr}} + \frac{C_c}{C_{cr}} + \frac{C_A}{C_{cr}}$$

where

$\dfrac{C_s}{C_{cr}}$ \qquad structural damping ratio

$\dfrac{C_c}{C_{cr}}$ \qquad control-system damping ratio

$\dfrac{C_A}{C_{cr}}$ \qquad aerodynamic damping ratio

The remaining terms are associated with the random aerodynamic loading. The function $\hat{C}_{L,n}(k_n)$ is the correlation function of the random section lift coefficients for the nth mode. Although not mathematically exact, a convenient way of thinking of this function is that it is the power spectrum of an effective random aerodynamic coefficient in the nth mode. The quantities R, L, q, and V are, respectively, reference radius, vehicle length, free-stream dynamic pressure, and free-stream velocity.

The use of equation (1) for scaling buffet loads is readily apparent. Since $\hat{C}_{L,n}(k_n)$ would be the same for both a dynamically scaled aeroelastic

model and the full-scale vehicle, the total full-scale bending moment is related to the corresponding model value by the following expression:

$$\sigma^2(z_0)_{T,F} = \sum_{n=1}^{\infty} \left(\frac{l_F}{l_M}\right)^7 \left(\frac{\omega_F}{\omega_M}\right)_n \left(\frac{q_F}{q_M}\right)^2 \left(\frac{V_M}{V_F}\right) \left[\frac{\left(\dfrac{c_A}{c_{cr}}\right)_M + \left(\dfrac{c_S}{c_{cr}}\right)_M}{\left(\dfrac{c_A}{c_{cr}}\right)_F + \left(\dfrac{c_S}{c_{cr}}\right)_F + \left(\dfrac{c_c}{c_{cr}}\right)_F}\right] \sigma^2(z_0)_{n,M} \qquad (2)$$

where, from dimensional considerations, the model-to-full-scale damping relationship is given by

$$\left(\frac{c_A}{c_{cr}}\right)_F = \left[\left(\frac{\rho_F}{\rho_M}\right)\left(\frac{V_F}{V_M}\right)\left(\frac{l_F}{l_M}\right)^2 \left(\frac{w_M}{w_F}\right)\left(\frac{f_M}{f_F}\right)\right]\left(\frac{c_A}{c_{cr}}\right)_M \qquad (3)$$

Although the full-scale bending moment at a particular location along the vehicle can be determined directly from equation (2), the missile or launch vehicle designer needs to know the distribution of bending moments along the structure. Therefore, in making dynamic bending-moment measurements on a model using a single strain-gage bridge, a strain-gage-location sensitivity factor must be determined since a bridge located say at the point of maximum bending moment in the first mode may not be very sensitive to moments produced by response in the second mode. This factor can be determined by calculating the bending-moment distribution due to inertia loading for motion in each mode, respectively.

Application of Buffet Bending-Moment Scaling Relationships

As an example of the technique, consider its application to an 8-percent dynamically scaled aeroelastic buffet model of the Saturn-Apollo launch configuration (built by the Los Angeles Division of North American Aviation for the NASA) that was tested recently in the transonic dynamics tunnel at the Langley Research Center. The Mach 1 point on the trajectory was chosen as the design point. The full-scale trajectory conditions and the tunnel performance capability and size dictate the model-to-full-scale design scaling ratios. The model design concept is shown in figure 10 which is a photograph of a portion of the model.

The backbone of the model was an 8-inch-inside-diameter central aluminum tube the thickness of which provided the properly scaled stiffness distribution (except for minor deviations because of model structural considerations) and the necessary strength to resist the loads imposed during testing. Lead weights attached to the aluminum tube provided the proper weight distribution. The aluminum tube and lead weights were covered by styrofoam segments which provided the correct external contour. The model was mounted in the tunnel on the support system described previously and shown in figures 3 and 4. The completed model, shown in figure 11, mounted in the Langley Research Center transonic dynamics tunnel was approximately $14\frac{1}{2}$ feet long and weighed about 786 pounds.

12

The primary instrumentation on the model consisted of several electric resistance-type strain-gage bridges bonded to the aluminum tube and calibrated to indicate bending moments. The gage outputs were recorded on tape during the tests. An accelerometer at the point of application of the shaker force to the model was used in conjunction with the shaker force output to determine the structural and aerodynamic damping.

In order to scale up the model test results to full-scale values using equation (2), it is first necessary to determine the relative contribution of each natural mode to the total bending moment measured on the model at a particular location. This can be accomplished by integrating the power spectra in the neighborhood of the resonant frequency of the desired mode. A typical bending-moment power spectrum for this model is shown in figure 12. Note that for this case, the first three free-free bending modes contribute to the total power.

The damping in a given vibration mode can be determined from the single-degree-of-freedom relationship for a distributed mass system: at resonance, damping is equal to the applied force multiplied by the normalized deflection at the point of application of the force and divided by the velocity of the point of normalization that is in phase with the applied force. (See, for example, ref. 8.) An electronic transfer function analyzer was used to measure these quantities. The model aerodynamic damping ratios $\left(\dfrac{c_A}{c_{cr}}\right)_M$ were determined by measuring the total damping with wind on and subtracting from that value the structural damping determined with the wind off. Full-scale aerodynamic damping was obtained from the model aerodynamic damping by the relation given in equation (3). An example of full-scale aerodynamic damping data is presented in figure 13 as the variation of the ratio of aerodynamic damping to critical damping with flight time for the first three free-free bending modes of the Saturn-Apollo launch vehicle. In this figure and in subsequent data figures concerning the Saturn-Apollo vehicle, values of damping and bending moments have been omitted in order to avoid a confidential classification. The values of damping shown in figure 13 are small, however. The maximum values are less than the estimated sum of the full-scale structural and control-system damping. The solid portion of the curves represents the range of the wind-tunnel studies for the model (M = 0.90 to M = 1.2). The dashed portions of the curves are estimated values. The peaks at M = 1.2 are caused primarily by the parameter ρV which diminishes rapidly after about 60 seconds of flight.

The full-scale bending moments for a particular mode at the point of measurement were then used in conjunction with the calculated bending-moment distribution due to the inertia loading to obtain the buffet bending-moment distribution in that mode. Figure 14 is an example of the distributed root-mean-square bending moment in the first three free-free modes. The data are for zero degrees angle of attack at the M = 0.9 point on the trajectory.

The mean-square buffet bending moments at each station for the various modes were then added to obtain the total bending-moment distribution. The final result is shown in figure 15 where the total root-mean-square buffet bending-moment distribution is presented for zero and 6° angle of attack.

Based on tests on the model with a "Jupiter" nose-cone payload with and without fins, it is felt that some of the measured model response may have been due to tunnel turbulence, and due to buffet load input from the relatively thick fins. Further investigations concerning these factors are in progress. Although no full-scale flight data are yet available for comparison with the predicted bending moments, definite plans have been made to attempt to obtain relevant full-scale data during the forthcoming SA-5 launch.

PREDICTION OF GROUND-WIND LOADS

Considerations in the Use of Models for

Ground-Winds Loads Prediction

As shown in figure 16, a launch vehicle erected on its pad or on a transporter prior to launch is subjected to a variety of loading conditions imposed by variable surface winds during those periods in which the protective gantry is removed. A steady wind imposes both a steady load due to aerodynamic drag and oscillatory loads due to flow separation or vortex shedding around the vehicle. These oscillatory loads are greatest in the plane perpendicular to the surface wind direction. Additional unsteady loads are caused by gusts and turbulence in the ground-wind flow. These ground-wind loads create problems in structural strength, guidance alinement, and ground handling; in fact, they are frequently the design loads for the lower stages of launch vehicles. The basic problem is to insure that the vehicle free-standing on the launch pad or transporter can satisfactorily withstand the ground wind specified for completion of the mission. For some missions this wind may be the 99.9-percent probable maximum wind during the month of highest winds at the launch site (see ref. 10).

Although considerable effort has been expended in study of the problem (see refs. 11 through 13), no satisfactory theoretical method exists for predicting the loads due to vortex shedding from ground winds on launch vehicles. Preliminary estimates of the oscillatory loads from vortex shedding may be made using a method described by Ezra (ref. 14) provided wind-induced response data are available for a vehicle of similar size and geometry. An alternate method based on unsteady pressure distributions was developed by Bohne (ref. 15). Such methods are useful for preliminary design purposes.

The best present means of obtaining quantitative data on ground-wind loads on launch vehicles, once the design is finalized, is from wind-tunnel studies of dynamically and elastically scaled models. Photographs of a number of typical ground-winds models tested in the Langley transonic dynamics wind tunnel are presented in figures 17(a) through 17(e). Notice the presence of the umbilical or service tower in most of these figures. If such a structure remains near the vehicle, it should be geometrically simulated because of its significant effect on the flow of ground winds over the vehicle.

There are uncertainties in the use of aeroelastic model wind-tunnel techniques for predicting ground-wind loads. The wind tunnel presents a steady wind of constant velocity profile without gusts and with a scale of turbulence different from atmospheric turbulence. Thus an adjustment must be

made for the difference between the actual velocity profile of atmospheric surface winds and the constant velocity profile of the wind tunnel. Also theoretical means such as Bohne's analysis in reference 16 must be used to determine the dynamic loads due to atmospheric turbulence and gusts. The aeroelastic models in the wind tunnel give the steady-state response of the vehicle due to ground winds and most importantly give the oscillatory response due to vortex shedding. In such tests, scatter in the dynamic response data is often present even though the test conditions are closely controlled. It has been found that vortex shedding has a stong three-dimensional end effect such that minor changes in shape or surface condition near the nose of the vehicle often have large effects on the response (see refs. 19 through 26). Therefore the model must reflect the geometry of the full-scale vehicle in great detail in the upper stages and nose regions of the model.

Scaling of Models

The dynamic response of the models to the random load inputs is in the model fundamental mode. This is illustrated in figure 18 by the power spectral density of the bending-moment response of a typical launch vehicle model to wind-tunnel simulated ground winds. Examination of response spectra of several models and of the full-scale Scout vehicle indicates this result is typical in that there is a single peak in the response at the fundamental frequency and virtually no response at higher frequencies. Such response is typical of the response of a lightly damped mechanical system to a random input (see ref. 27).

Just as for the case of the buffet-type model, scaling laws based on the response of mechanical systems to random inputs (refs. 14 and 27) are used to determine the nondimensional parameters to be duplicated by the model if the response of the model to tunnel-simulated ground winds is to simulate accurately the response of the full-scale vehicle to ground winds. It is required that the following parameters be the same for model and full-scale vehicle:

1. External shape

2. Reynolds number $\rho V l / \mu$

3. Reduced frequency $f_n l / V$ where f_n is natural frequency of nth mode (n = 1, 2)

4. Mass ratio $M_n' / \rho l^3$ where ρ is mass density of test medium and M_n' is generalized mass of nth mode (n = 1, 2)

5. Damping ratio C_s / C_{cr} where C_s is structural damping and C_{cr} is critical damping

6. Surface roughness ratio ϵ / l where ϵ is surface roughness height per representative length

From the dimensionless parameter design requirements just specified and from a knowledge of the wind-tunnel capabilities, the fundamental scale factors

(model-to-full-scale ratios) for scaling model length, mass, and time are readily obtained. The scale factors for any other physical parameter is obtained by substituting in the dimensional expression for the desired parameter the value of the model scale factors for length, mass, and time.

As mentioned in the introduction, the primary flow parameter to be simulated for ground-wind models is Reynolds number. The primary flow variable for buffet models, Mach number, is of importance in ground-wind model work only because the tunnel Mach number must not exceed 0.4 if compressibility effects not present in atmospheric ground winds are to be avoided. This Mach number limitation and the design requirement that full-scale Reynolds number shall be simulated combine to limit the range of ground winds which can be simulated in the wind tunnel. Figure 19 shows for several launch vehicles the ground-wind velocity simulation which can be obtained under these restrictions in the Langley transonic dynamics wind tunnel which is a large, variable-density wind tunnel with an approximately 16-foot-square test section. For large vehicles such as Saturn V and Nova the ground-winds simulation range is far lower than design ground-wind values.

A tentative solution to this problem is to change the design restriction that full-scale Reynolds number shall be simulated to a design restriction that the Reynolds number on both model and full-scale vehicle shall be supercritical ($R_N > 500,000$) for the ground-wind velocities of interest. The assumption is that the flow simulation is adequate if the model Reynolds numbers are supercritical although less than full-scale Reynolds number. This technique has been used for Titan III and Saturn V models to enable higher ground-wind velocities to be simulated. Full-scale data to test the validity of the results are not yet available.

Model Construction and Mounting

The model construction usually follows one of two techniques frequently used in dynamic model design. One technique uses a metal outer shell of varying thickness. This shell forms the basic exterior shape of the vehicle and simulates the stiffness distribution along the longitudinal axis. Additional weights required to simulate the vehicle weight distribution along the longitudinal axis are attached to the interior of the stiffness carrying shell in such a manner that they do not contribute significantly to the bending stiffness. The other technique involves a center beam or spar of varying cross section along the longitudinal axis which provides the correct scaled bending stiffness along the longitudinal axis. This central spar is surrounded by a low stiffness material which gives the correct external shape and has imbedded weights to provide the correct scaled mass distribution.

Structural damping in the model (C_S) has in the past been difficult to control as accurately as other design parameters. If the model damping differed from that of the full-scale vehicle, scaling corrections are made in the data in accordance with the scaling relationships in reference 14 which show that the model response varies inversely with the square root of the structural damping. There has recently been developed by Mr. Wilmer H. Reed III of the Langley Research Center a viscous damper suitable for installation on ground-winds models such as we are discussing. Figure 20 shows the construction of the damper. A cylinder filled with viscous oil has

a number of lead discs resting on concave trays in the cylinder. As the model oscillates perpendicular to its longitudinal axis, the combined action of the fluid and lead weights provides a means for energy dissipation. The damper is mounted as shown in the upper stage of the vehicle. By varying the viscosity of the oil or the weight of lead discs, various values of structural damping can be obtained. On its initial test on a model whose structural damping was approximately 0.007 without the damper installed, controlled variations in damping from 0.01 to 0.03 were obtained with the use of the damper. The damper promises to be very useful in the initial and future tests.

The models are mounted at the station corresponding to the full-scale vehicle tie-down station on a base mount fixture designed to simulate the scaled tie-down stiffness of the full-scale vehicle. Since at the time of model testing, an accurate value of full-scale tie-down stiffness is often not known, a variable stiffness base mounting fixture has been developed which is shown in figure 21. The fixture has a center cylinder with heavy flanges on either end. The center cylinder supports the model weight and has a value of stiffness somewhat lower than the scaled tie-down stiffness should be. Eight pretensioned steel rods with or without cylindrical sleeves can be fastened between the upper and lower flanges to increase the stiffness of the fixture. By varying the diameter of the peripheral rods, differen values of tie-down stiffness may be obtained. The model is attached by bolts to the upper flange. The lower flange bolts to a massive 8-foot-diameter turntable which may be rotated from the control room to any desired wind azimuth angle. Desirable features of this variable stiffness base mounting fixture are that it has repeatable values of stiffness which can be changed without dismounting the model, and its design and fabrication are simple.

Instrumentation

The primary instrumentation for measuring model response consists of two strain-gage bridges mounted near the model base station in planes 90° apart around the circumference and two accelerometers mounted on the model near the nose in the same two reference planes. These sensors are used to obtain time histories of the bending-moment and deflection responses of the model to simulated ground winds. Conventional readout instrumentation such as recording oscillographs, oscilloscopes, and thermocouples (for mean square of response) are used.

One interesting component of readout instrumentation which has been developed for the ground-wind tests is the use of time exposure photographs of an oscilloscope set up to display the response from one bending-moment strain gage on one axis and the response from the strain gage in the other reference plane on the other axis. Figure 22 shows this arrangement schematically. A no-wind position spot shows no-load position. As the model responds both statically and dynamically, the outputs from these strain gages trace an elliptical pattern on the oscilloscope since the lift response is greater than the drag response. The borders of the ellipse thus formed represent the curve of maximum dynamic bending-moment response during a data sample and the distance the center of the ellipse has shifted from the no-wind spot gives the magnitude and direction of the static bending-moment response. The maximum length vector which can be drawn from the wind-off zero spot to the outside of the dynamic-response envelope is the maximum resultant bending moment. An

excellent feature of this type of presentation is that it has the correct relationship between the maximum oscillatory response in the lift and drag directions.

Tests and Results

The usual procedure in ground-wind tests is to set the tunnel at a constant velocity which simulates a sizable ground wind and then rotate the model and umbilical tower through 180° or 360° of wind azimuth angle, stopping at various azimuth angles to record 1- or 2-minute data samples of the model response. The time scale factor is such that 1- or 2-minute model data samples represent many minutes of full-scale data. Due to the presence of the umbilical tower or asymmetries in the model, there are usually one or more wind azimuth angles for which the response is larger than at other angles. This variation of the response with wind azimuth angle is strikingly shown in figure 23 by the oscillograph time histories taken at a constant velocity but varying wind azimuth angle. The model and umbilical tower are represented schematically in top view in the center of the figure. The five wind azimuth angles are shown by the broad arrows and the oscillograph response for each wind angle is opposite the point of the arrow. It is readily seen that the wind flow through the umbilical tower affects the model response with the maximum response at 135°. Note that the steady-state vector has a lift as well as a drag component which is believed to be caused by the partial blockage of one side of the umbilical tower by a series of conduit cable shields.

Once the wind azimuth angles of greatest response are determined, the variation of model response with simulated ground-wind velocity is determined for each of these angles over a range of simulated ground winds up to the $M = 0.4$ compressibility limit.

Typical plots of the constant velocity, variable wind azimuth response and constant azimuth, variable ground-wind responses are shown in figure 24. The base bending-moment response is plotted against turntable angle in the upper figure for a simulated velocity of 40 knots and the base bending response of the maximum response wind azimuth angle of 135° is shown in the bottom figure as a function of tunnel dynamic pressure which varies as the square of simulated ground-wind velocity.

Application of Model Data to Full-Scale Vehicle

By use of the scale factors derived for the model, the model ground-wind response measured in the wind tunnel can be scaled to the full-scale vehicle. These data give the loads on the model imposed by a uniform stream velocity, namely (a) steady drag and lift loads and (b) unsteady loads associated with vortex shedding due to flow separation. Modifications must be made to the wind-tunnel measured loads to account for differences between the uniform velocity in the wind tunnel and the parabolic velocity gradient near the ground in the atmosphere. In addition, the response from unsteady loads due to gusts and turbulence found in atmospheric winds but not present in the tunnel flow must be calculated.

The modification of tunnel test data for velocity profile shape is accomplished by finding an equivalent uniform velocity U_e which distributed along the vehicle gives the same steady-state bending moment at the base as the design ground-wind profile.

Two approaches may be used to estimate the unsteady loads on the vehicle caused by gusts and turbulence in the atmosphere. The first approach assumes the wind input to be in the form of a discrete gust tuned to the vehicle natural frequency. The other approach assumes the wind input from gusts and turbulence can best be represented by the statistical properties of a stationary random process (see, for example, ref. 16). The second approach more realistically represents the effects of structural damping and is the one favored herein. Components of velocity (from gusts and turbulence) in the direction of and perpendicular to the wind direction are considered. In this approach the components of the velocity fluctuations due to gusts and turbulence are assumed to be random functions of time perfectly correlated along the vehicle length. Aerodynamic loads are defined by a two-dimensional strip analysis. An equivalent uniform velocity profile is used. The equations of motion are linearized. The dynamic model response is assumed to occur in the fundamental mode. A specific power spectrum for atmospheric turbulence developed by Von Karman (ref. 17) and applied by Houbolt (ref. 18) is used. A scale of turbulence is assumed and the intensity of turbulence is specified such that the 3σ level of the turbulence velocity components corresponds to $0.4U_e$, the amount by which the peak design wind exceeds the mean equivalent wind U_e. The envelope of the 3σ bending-moment response due to turbulence and gusts calculated from the preceding assumptions is an ellipse similar to that for maximum dynamic response due to vortex shedding except the major axis is in the plane of the wind.

The equivalent velocity profile U_e, and the 3σ turbulence-response envelope, both calculated as described, are combined with the steady-state response and response due to vortex shedding, both measured in the wind tunnel. The method of combining these loads to get a final answer for the full-scale vehicle response to ground winds is shown in figure 25. In this figure the input winds are the equivalent velocity U_e plus the u and v components of atmospheric turbulence and gusts. The 3σ turbulence response envelope has its center at the end of the steady drag vector. The vortex shedding response envelope is moved with its center on the boundary of the turbulence-response envelope to establish a locus of points from which the maximum resultant base bending moment may be determined.

At present there are little or no full-scale data available to verify the assumptions in this analysis and the data from ground-wind model in wind-tunnel tests. However, preparations are currently being made for erecting surplus Jupiter and Thor vehicles at Wallops Island for obtaining full-scale ground-winds data. Ground-wind full-scale measurements on full-scale Saturn vehicles are also being planned.

REFERENCES

1. Coe, Charles F.: Steady and Fluctuating Pressures at Transonic Speeds on Two Space-Vehicle Payload Shapes. NASA TM X-503, 1961.

2. Coe, Charles F.: The Effects of Some Variations in Launch-Vehicle Nose Shape on Steady and Fluctuating Pressures at Transonic Speeds. NASA TM X-646, 1962.

3. Jones, George W., Jr., and Foughner, Jerome T., Jr.: Investigation of Buffet Pressures on Models of Large Manned Launch Vehicle Configurations. NASA TN D-1633, 1963.

4. Doggett, Robert V., Jr., and Hanson, Perry W.: An Aeroelastic Model Approach for the Prediction of Buffet Bending Loads on Launch Vehicles. NASA TN D-2022, 1963.

5. Coe, Charles F.: The Effect of Model Scale on Rigid-Body Unsteady Pressures Associated With Buffeting. Presented at the Symposium on Aeroelastic and Dynamic Modeling Technology, Dayton, Ohio, September 23-25, 1963.

6. Rice, S. O.: Mathematical Analysis of Random Noise. Pts. I and II, Bell System Tech. Jour., Vol. XXIII, No. 3, July 1944, pp. 282-332; Pts. III and IV, Vol. XXIV, No. 1, Jan. 1945, pp. 46-156.

7. Liepmann, H. W.: On the Application of Statistical Concepts to the Buffeting Problem. Jour. Aero. Sci., Vol. 19, No. 12, Dec. 1952, pp. 793-801.

8. Hanson, Perry W., and Doggett, R. V., Jr.: Wind-Tunnel Measurements of Aerodynamic Damping Derivatives of a Launch Vehicle Vibrating in Free-Free Bending Modes at Mach Numbers From 0.70 to 2.87 and Comparisons With Theory. NASA TN D-1391, 1962.

9. Hanson, Perry W., and Doggett, Robert V., Jr.: Aerodynamic Damping of a 0.02-Scale Saturn SA-1 Model Vibrating in the First Free-Free Bending Mode. NASA TN D-1956, 1963.

10. Daniels, Glenn E.: Natural Environment (Climatic) Criteria Guidelines for Use in MSFC Launch Vehicle Development. 1963 Revision MSFC MPT-AERO-63-9, Jan. 28, 1963. (Supersedes MPT-AERO-61-93.)

11. Fung, Y. C.: Fluctuating Lift and Drag Acting on a Cylinder in a Flow at Supercritical Reynolds Numbers. Jour. Aerospace Sciences, Vol. 27, No. 11, Nov. 1960, pp. 801-804.

12. Humphreys, J. S.: On a Circular Cylinder in a Steady Wind. Jour. of Fluid Mechanics, Vol. 9, Pt. 4, Dec. 1960, p. 603.

13. Roshko, Anatol: Experiments on the Flow Past a Circular Cylinder at Very High Reynolds Number. Jour. of Fluid Mechanics, Vol. 10, pt. 3, May 1961, pp. 345-356.

14. Ezra, A. A., and Birnbaum, S.: Design Criteria for Space Vehicles to Resist Wind-Induced Oscillations. Am. Rocket Soc. Paper 1081-60. Presented at the Structural Design of Space Vehicles Conf., Santa Barbara, Calif., Apr. 6-8, 1960.

15. Bohne, Quentin R.: Ground Wind-Induced Loads on Launch Vehicles. Tech. Doc. Rept. ASD-TDR-62-371, Aug. 1962.

16. Bohne, Quentin R.: Power Spectral Considerations on the Launch Pad. USAF Geophysics Res. Dir. A.F. Surveys in Geophysics., No. 140, Proc. of National Symposium on Winds for Aerospace Vehicle Design, Vol. 1, AFCRL-62-273(1), Mar. 1962.

17. Von Karman: Progress in Statistical Theory of Turbulence. (Paper 101, Anniversary Series, Vol. IV.)

18. Houbolt, John C., Steiner, Roy, and Pratt, Kermit G.: Flight Data and Consideration of the Dynamic Response of Airplanes to Atmospheric Turbulence. Presentation to the Structures and Materials Panel, Advisory Group for Aeronautical Research and Development, Paris, France, July 3-13, 1963. (To be published as an NASA TR.)

19. Buell, Donald A., and Kenyon, George C.: The Wind-Induced Loads on a Dynamically Scaled Model of a Large Missile in Launching Position. NASA TM X-109, Dec. 1959.

20. Young, J. P.: Wind-Induced Oscillation Tests of 1/6-Scale Pershing Model. The Martin Company Engineering Rep. No. 11461, Aug. 1960.

21. Rich, Roy L.: Preliminary Ground Wind Induced Oscillation Test, Dyna Soar, Step I. Boeing Aircraft Company Document No. D-2-8147, Aug. 1961.

22. Killough, T. L.: Wind-Induced Loads on a Dynamic 1/5-Scale Unfueled SM-78 Jupiter in the Launch Position (U). U.S. Army Ordnance Missile Command, Rep. No. RG-TM-62-65, July 10, 1962.

23. Cincotta, J. J., and Lambert, W. H.: Preliminary Report 7.5 Percent 624A Ground Wind and Wind-Induced Oscillation Wind Tunnel Tests (U). Martin Company, Mar. 1963, Contract No. AF-04(695)-150.

24. Farmer, Moses G.: Response to Simulated Ground Winds of a Dynamically and Elastically Scaled Model of the Unfueled Jupiter Missile in the Launch Position. Prospective NASA TM.

25. Jones, George W., Jr., and Farmer, Moses G.: Response to Ground Winds and Booster Static Pressure Distribution on a 0.075-Size Model of Saturn Block I (SA-1) Vehicle in Launch Configuration. Prospective NASA TM.

26. Buell, Donald A., McCullough, George B., and Steinmetz, William J.: A Research Investigation in the Ames 12-Foot Pressure Wind Tunnel of Wind-Induced Loads on Axisymmetric Missiles in Launch Position. Prospective NASA TM.

27. Thompson, W. T., and Barton, M. V.: The Response of Mechanical Systems
      to Random Excitations. Jour. Appl. Mech., Vol. 24, No. 2,
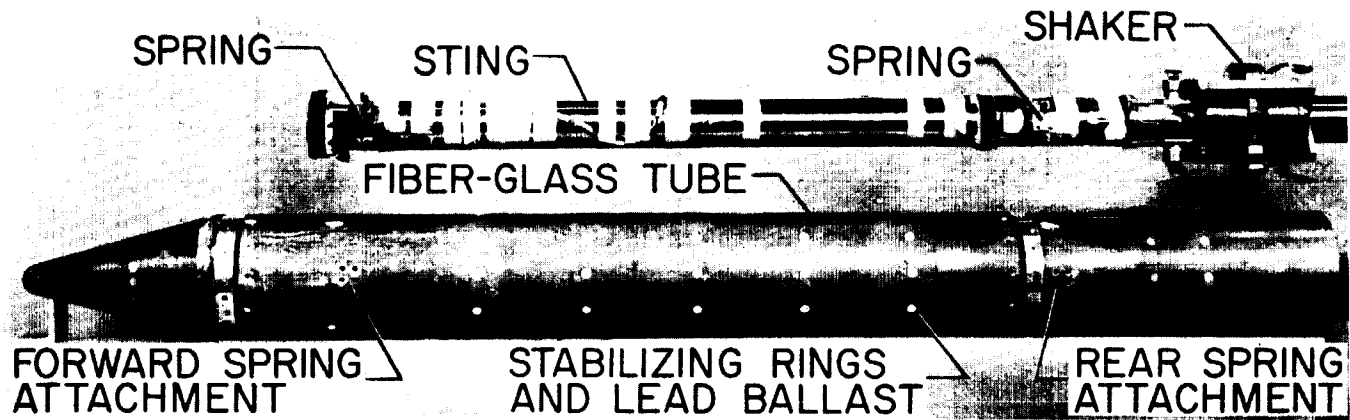   pp. 248-251, June 1957.

A-A

ON LAUNCH PAD

V

A   A

IN FLIGHT

V
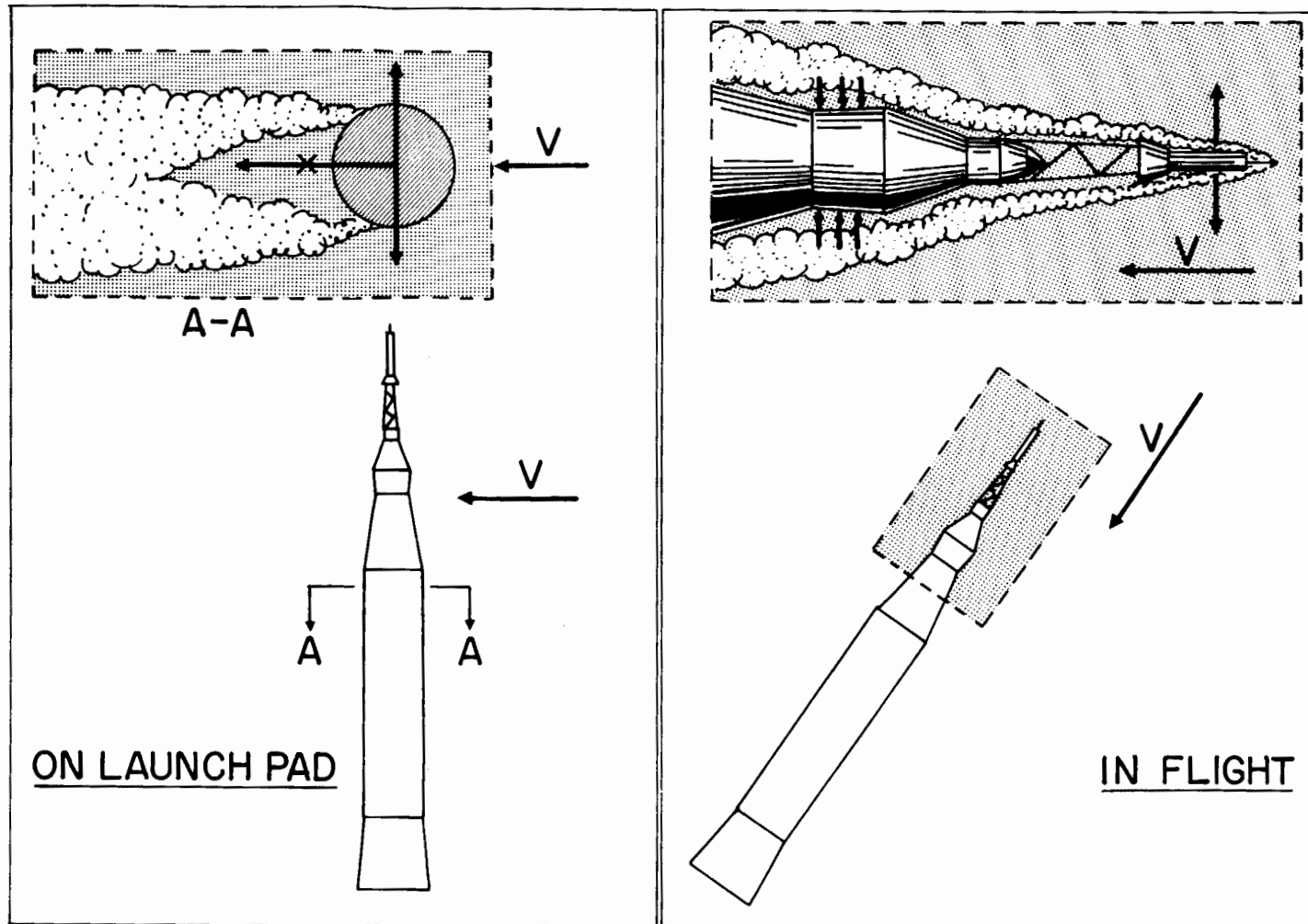
NASA

Figure 1.- Schematic illustration of loads caused by separated flow over a vehicle on launch pad and in flight.
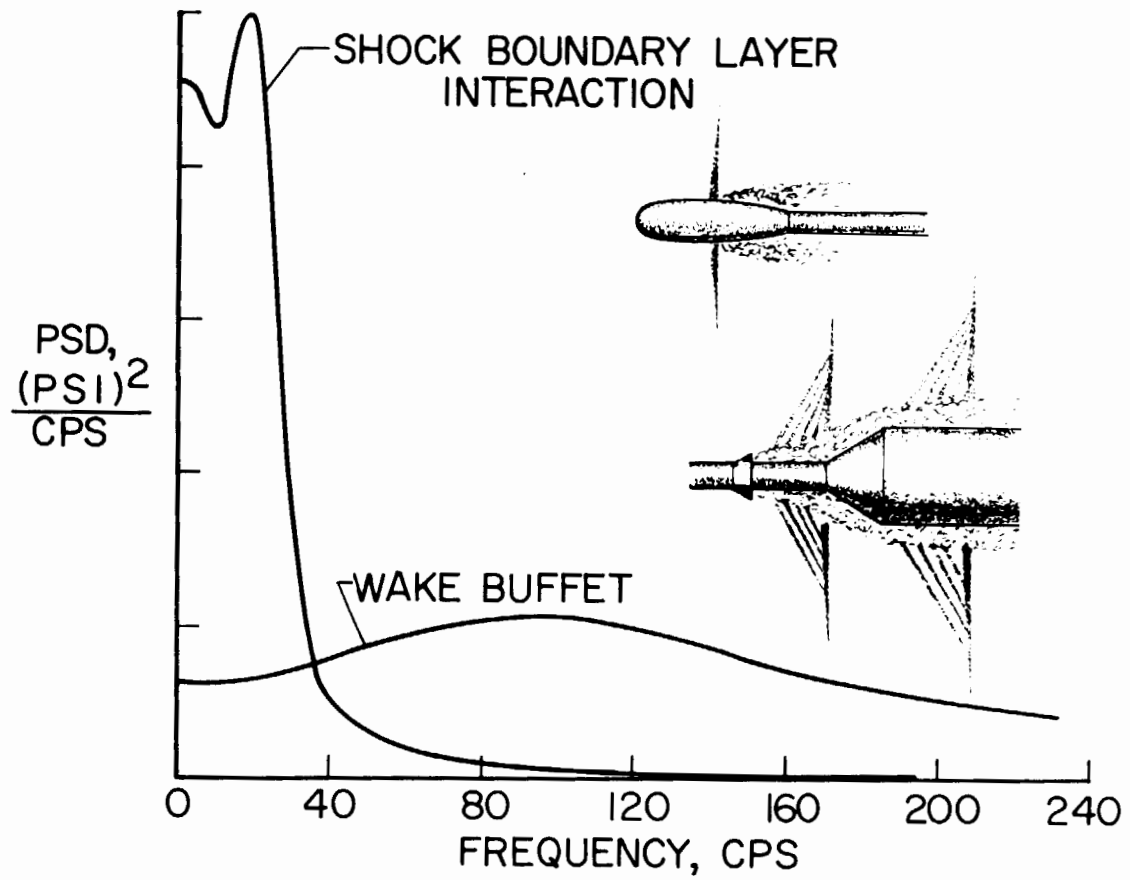
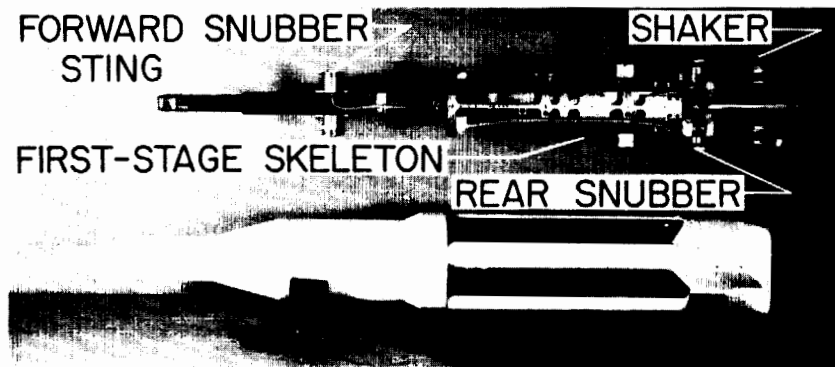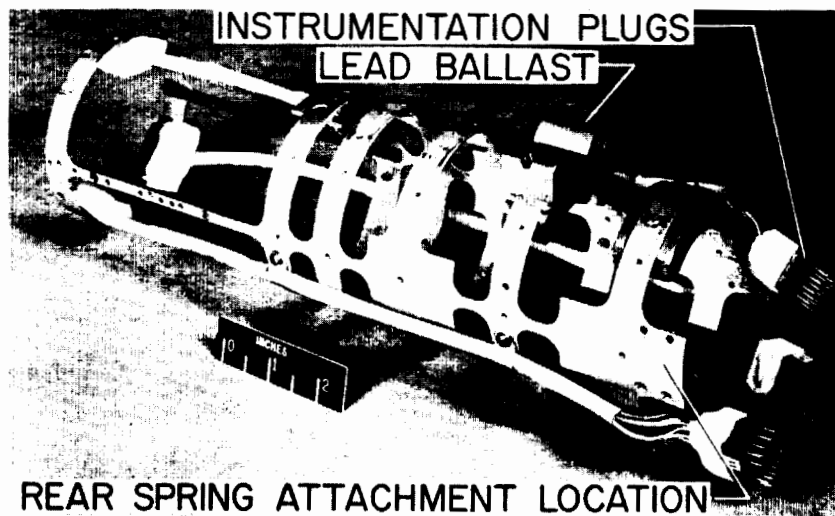Figure 2.- Pressure power spectra of two transonic buffet flows.

SPRING   STING   SPRING   SHAKER

FIBER-GLASS TUBE

FORWARD SPRING
ATTACHMENT   STABILIZING RINGS
AND LEAD BALLAST   REAR SPRING
ATTACHMENT

NASA
L-61-1191

Figure 3.- Simple aeroelastic model and sting.

25

FORWARD SNUBBER
STING

SHAKER

FIRST-STAGE SKELETON

REAR SNUBBER

(a) Assembled model shell with first-stage skeleton and   L-61-6021
electromagnetic shaker on sting.

INSTRUMENTATION PLUGS

LEAD BALLAST

REAR SPRING ATTACHMENT LOCATION

(b) Details of first-stage skeleton.

Figure 4.- Two-percent Saturn aeroelastic model.
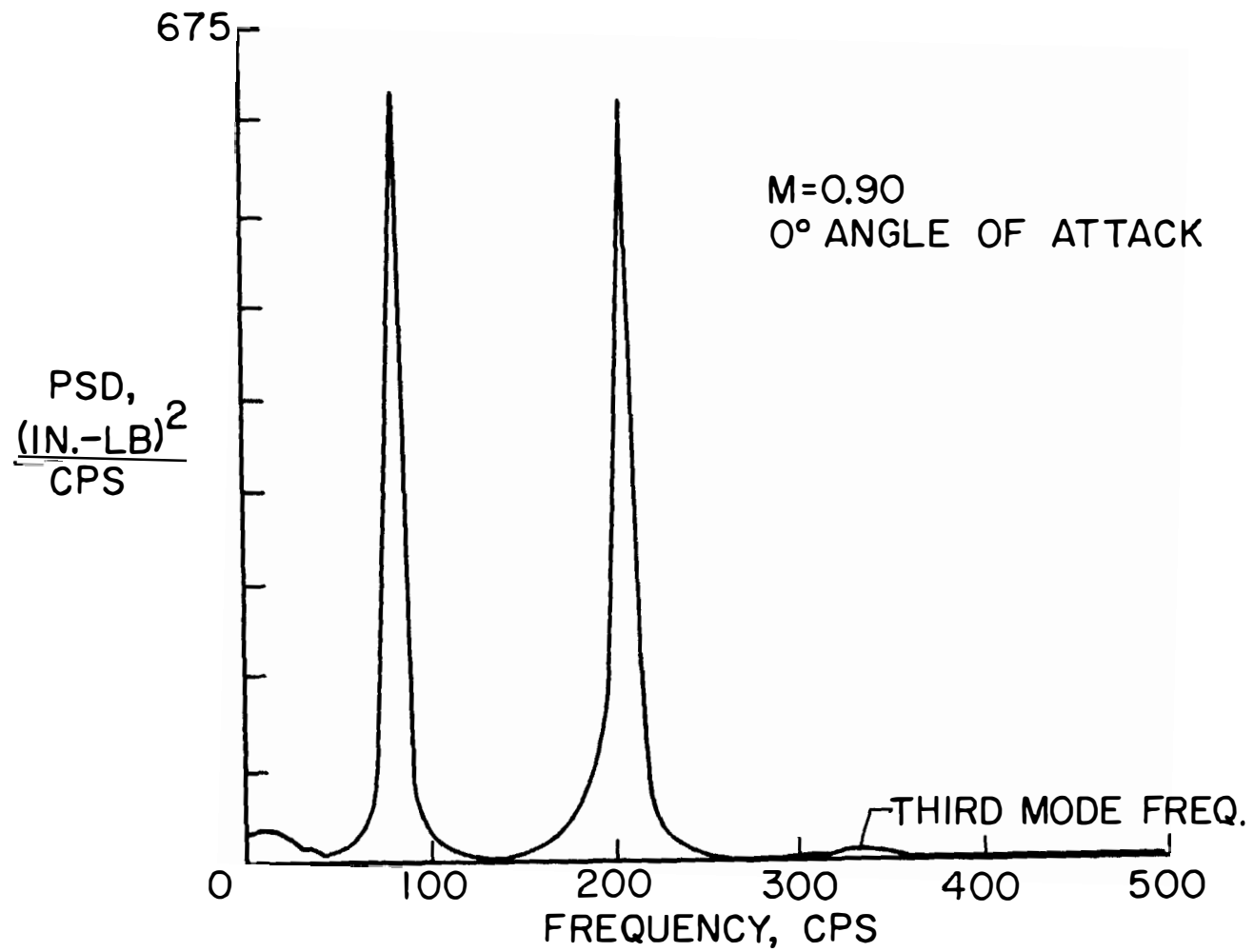
Figure 5.- Spectrum of bending-moment response of a "bulbous nose" configuration.

MODE SHAPES

EXP.	CALC.	MODE
O	————	1
□	————	2
△	—·—·—	3

FREQ., CPS

EXP.	CALC.	MODE
11.04	11.60	1
18.27	19.80	2
30.42	32.30	3
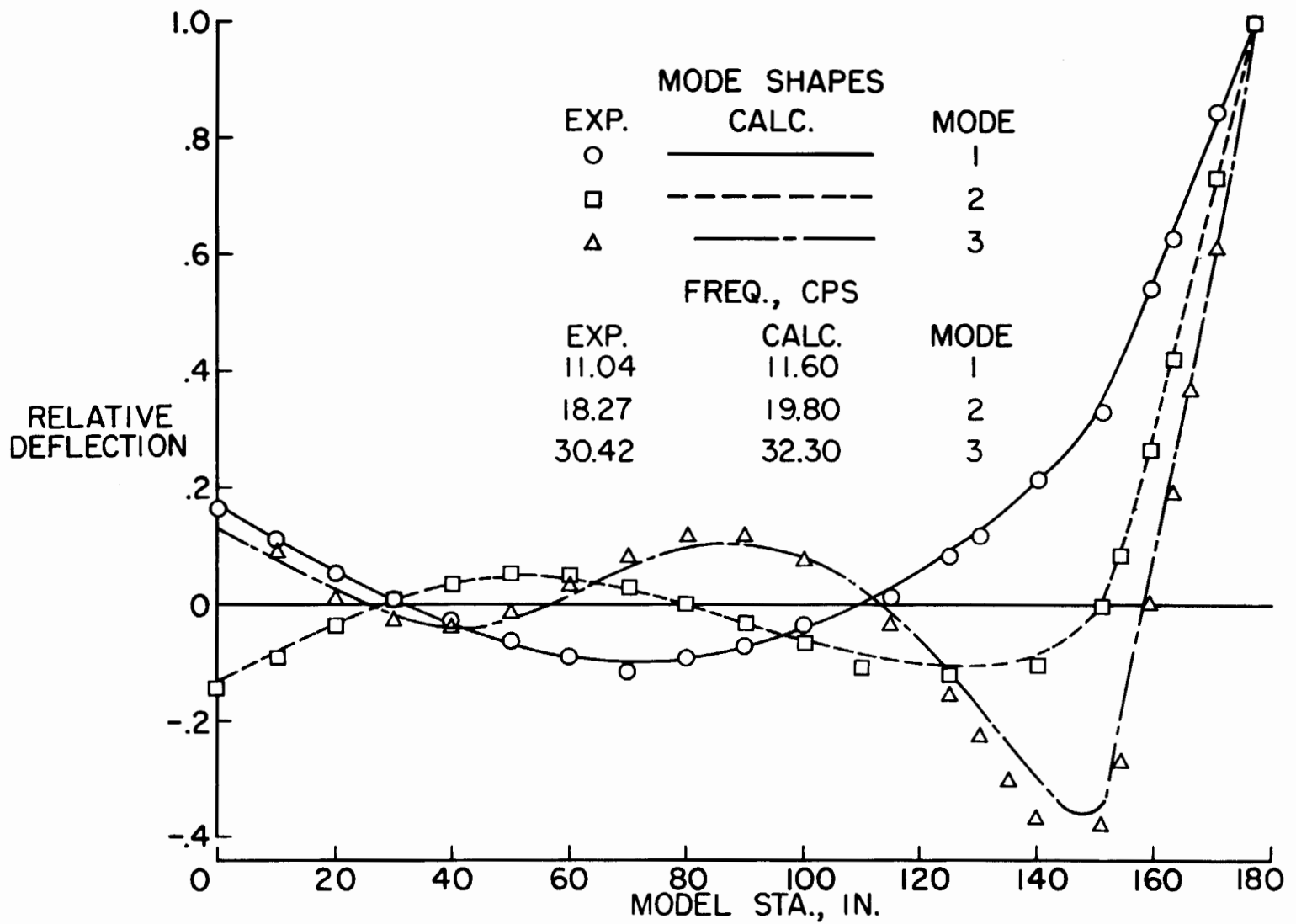
NASA

Figure 6.- Calculated free-free mode shapes and frequencies compared with measured mode shapes and frequencies of mounted model.

28

TORQUE SPRINGS MOUNTED EXTERNAL TO TEST SECTION

CABLES ATTACHED TO FORWARD AND REAR NODE POINTS AND ROUTED ALONG STING OUT REAR OF MODEL

V

FORWARD LEAF SPRING

STING

SINUSOIDAL FORCE FROM SHAKER

REAR LEAF SPRING

STING

DEFLECTED MODEL

MODEL UNDEFLECTED CENTERLINE
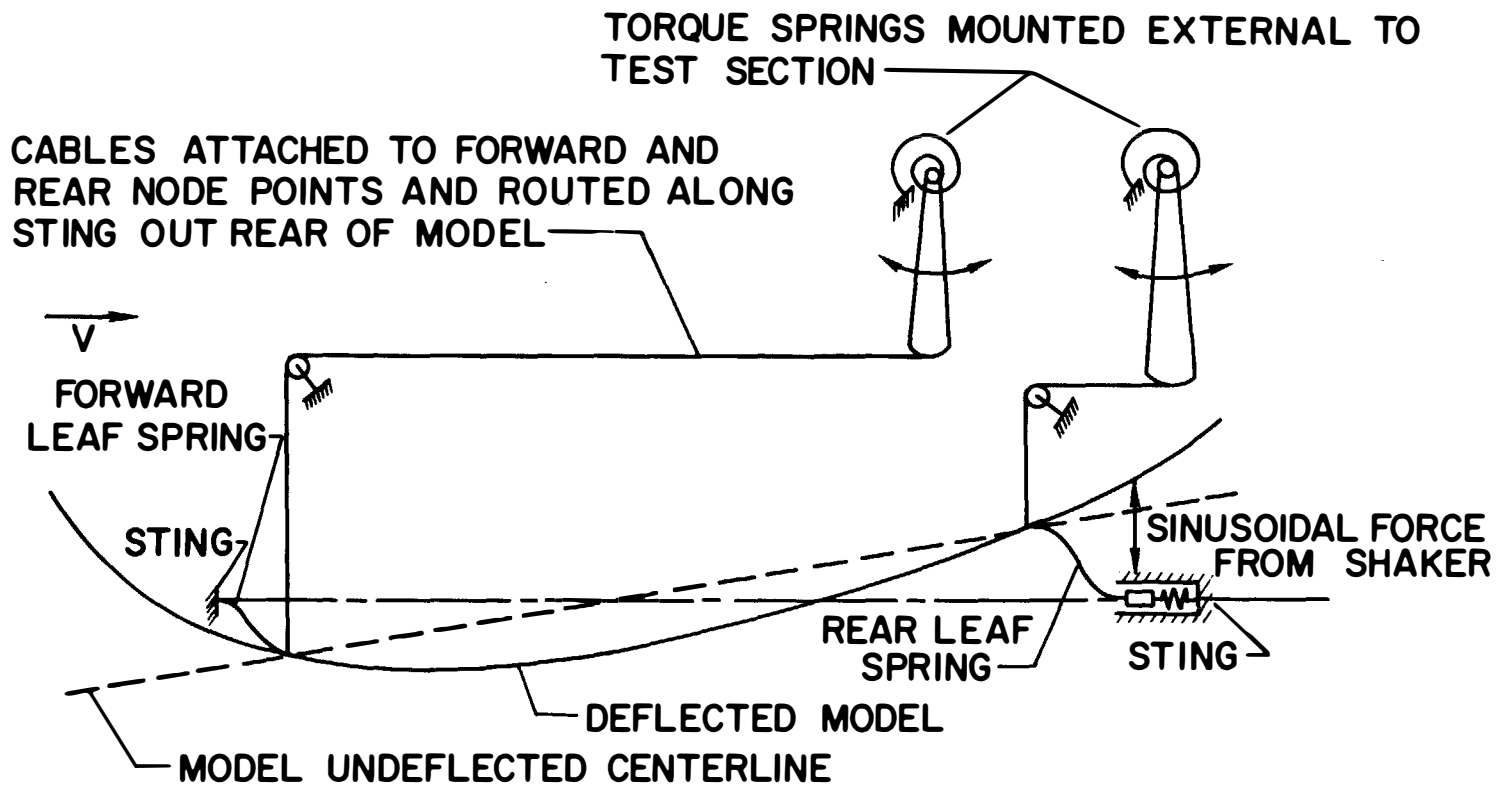
NASA

Figure 7.- Schematic diagram of aeroelastic buffet model support system.

ELECTROMAGNETIC SHAKER MOVING COILS

FIELD COILS

REAR LEAF SPRING

MODEL SNUBBER RETRACTED

MODEL SNUBBER EXTENDED

SUPPORT CABLE

FORWARD LEAF SPRING
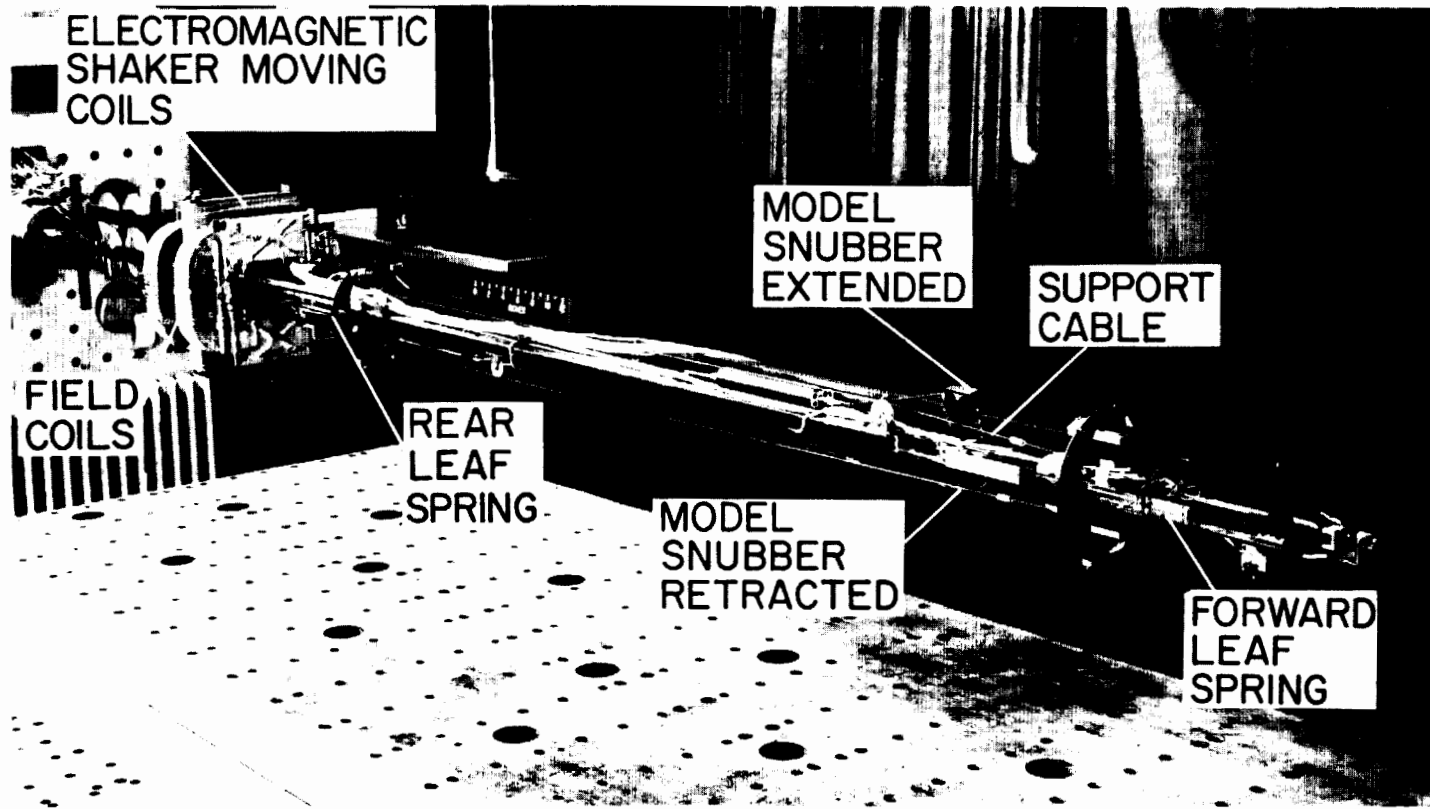
NASA
L-63-5842

Figure 8.- Photograph of sting used for testing 8-percent Saturn-Apollo buffet model.
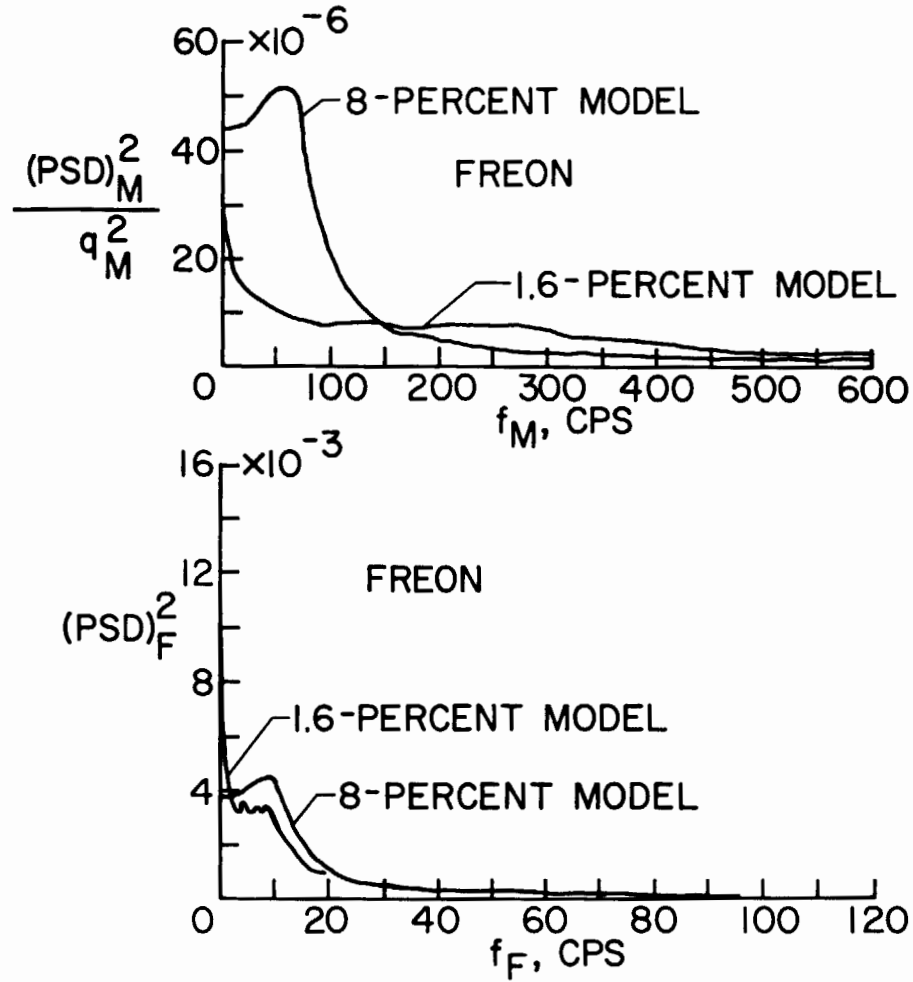
(a) Comparison of data at station "a" for 1.6- and 8-percent models   NASA
tested in Freon, M = 0.8.

Figure 9.- Evaluation of buffet scaling relationships as applied to rigid
fluctuating pressure models.
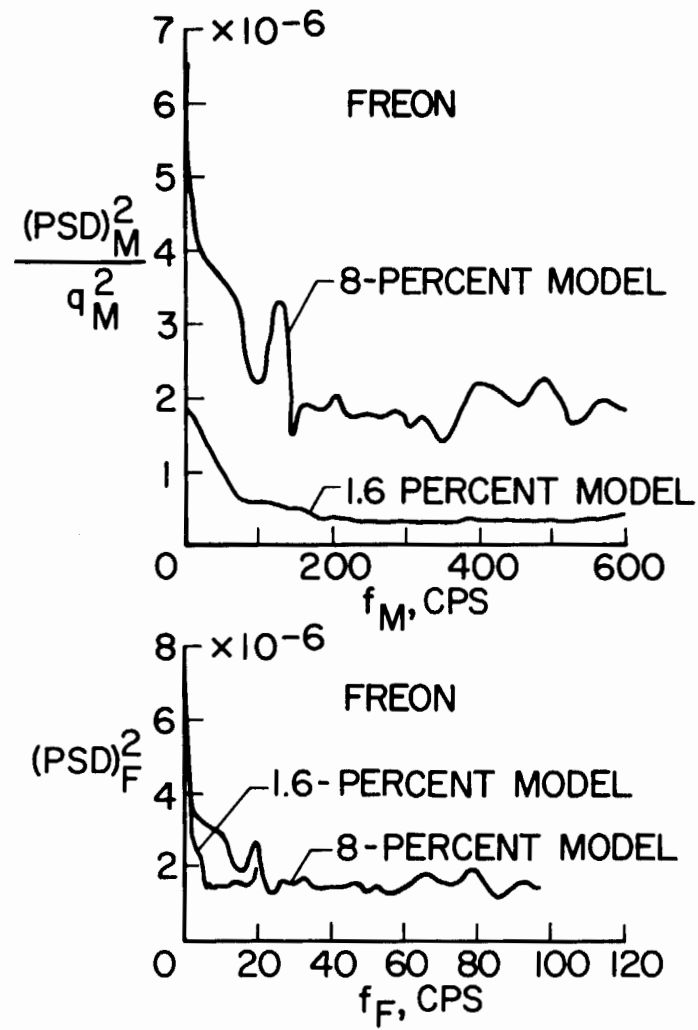
(b) Comparison of data at station "b" for 1.6- and 8-percent models   NASA
tested in Freon, M = 0.81.
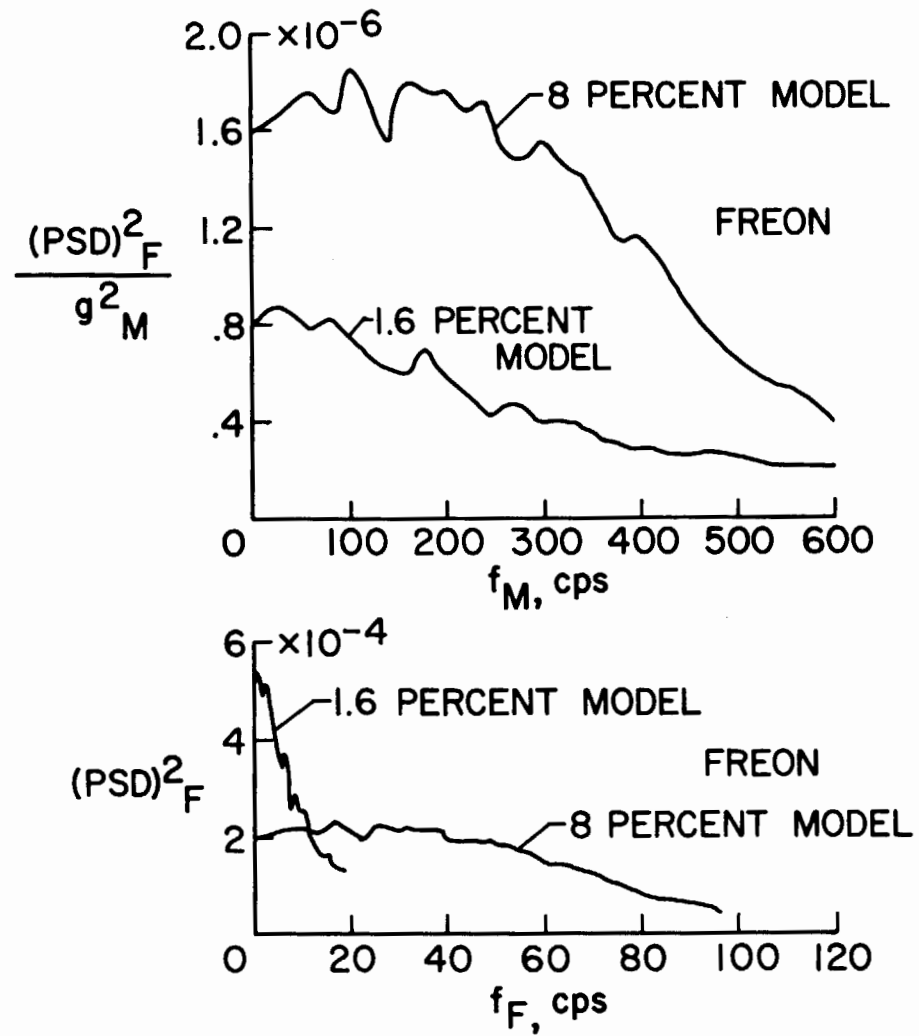
Figure 9.- Continued.

(c) Comparison of data at station "a" for 1.6- and 8-percent models tested in Freon, M = 1.01.

Figure 9.- Continued.

(d) Comparison of data at station "a" for 8-percent model tested in Freon and in air, M = 1.05.

NASA

Figure 9.- Continued.
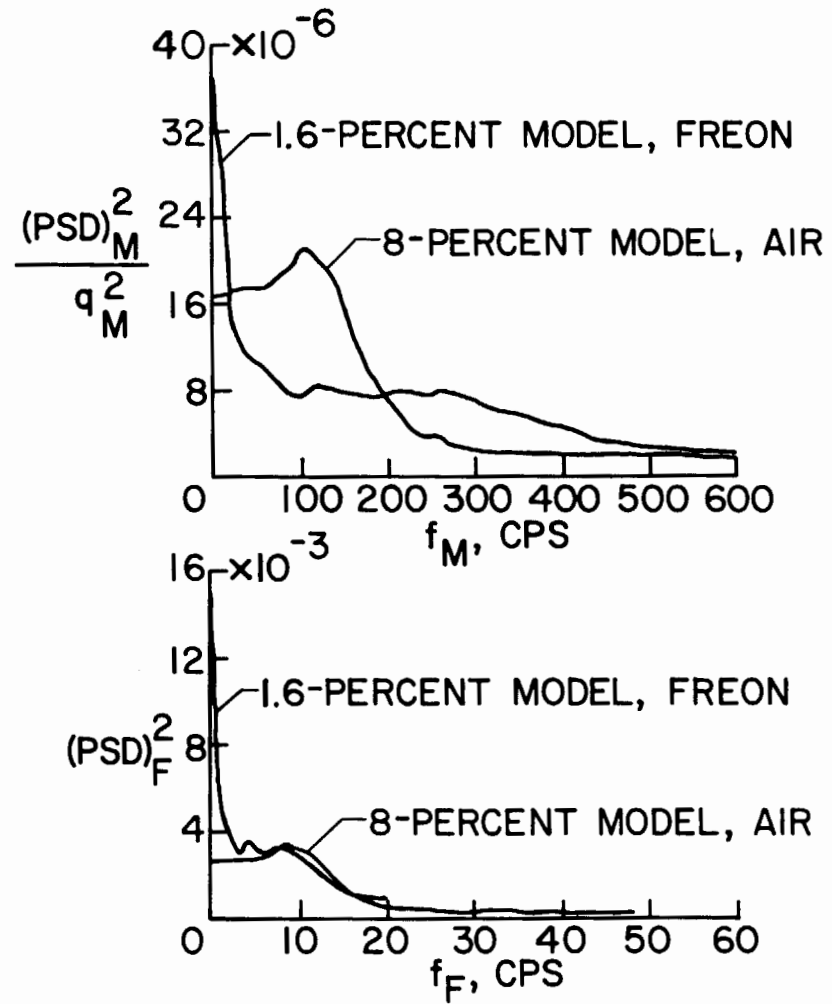
(e) Comparison of data at station "a" for 1.6-percent model tested in Freon and for 8-percent model tested in air, M = 0.8.

NASA

Figure 9.- Concluded.

ALUMINUM TUBE

LEAD
WEIGHT

STYROFOAM
SEGMENTS
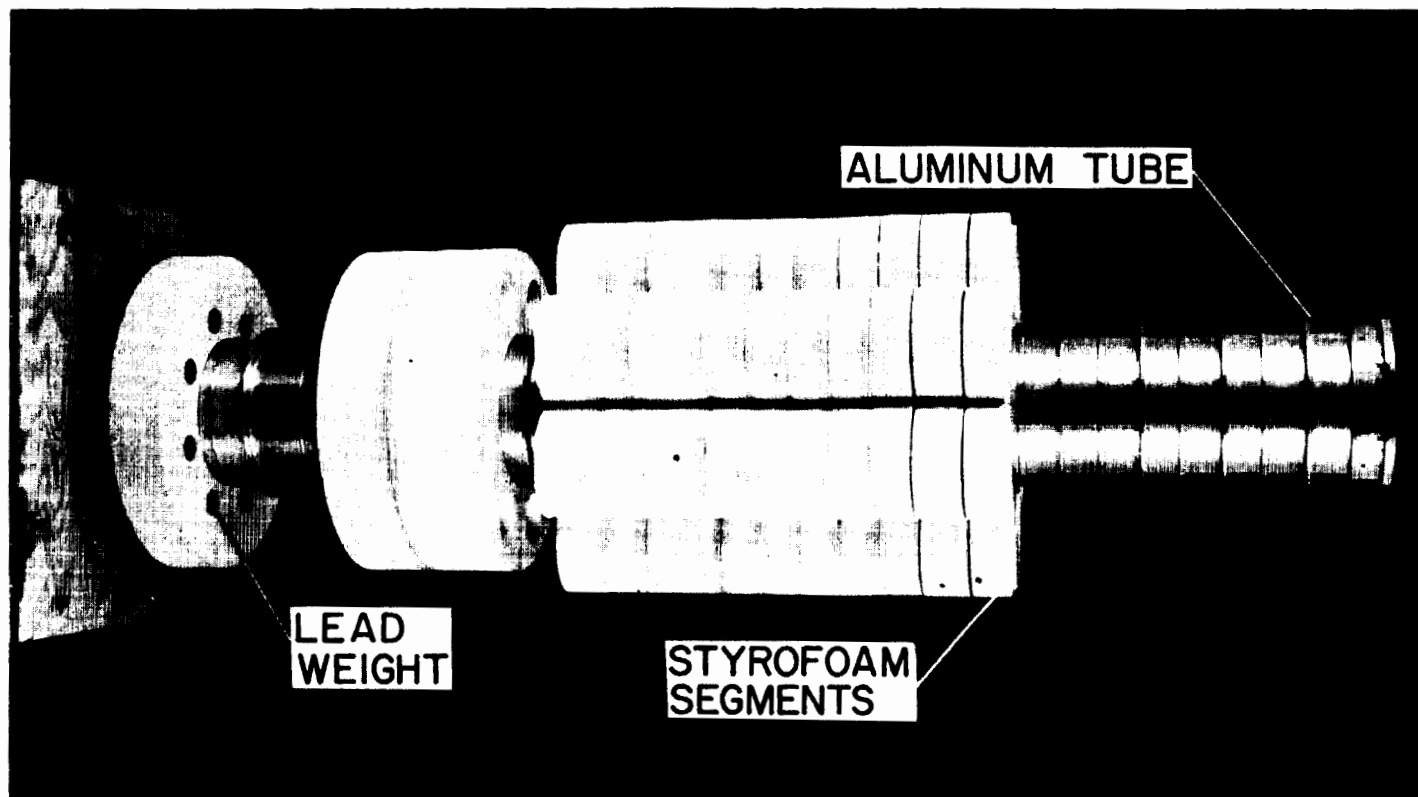
NASA
L-62-9403

Figure 10.- Portion of 8-percent Saturn-Apollo aeroelastic buffet model.

36
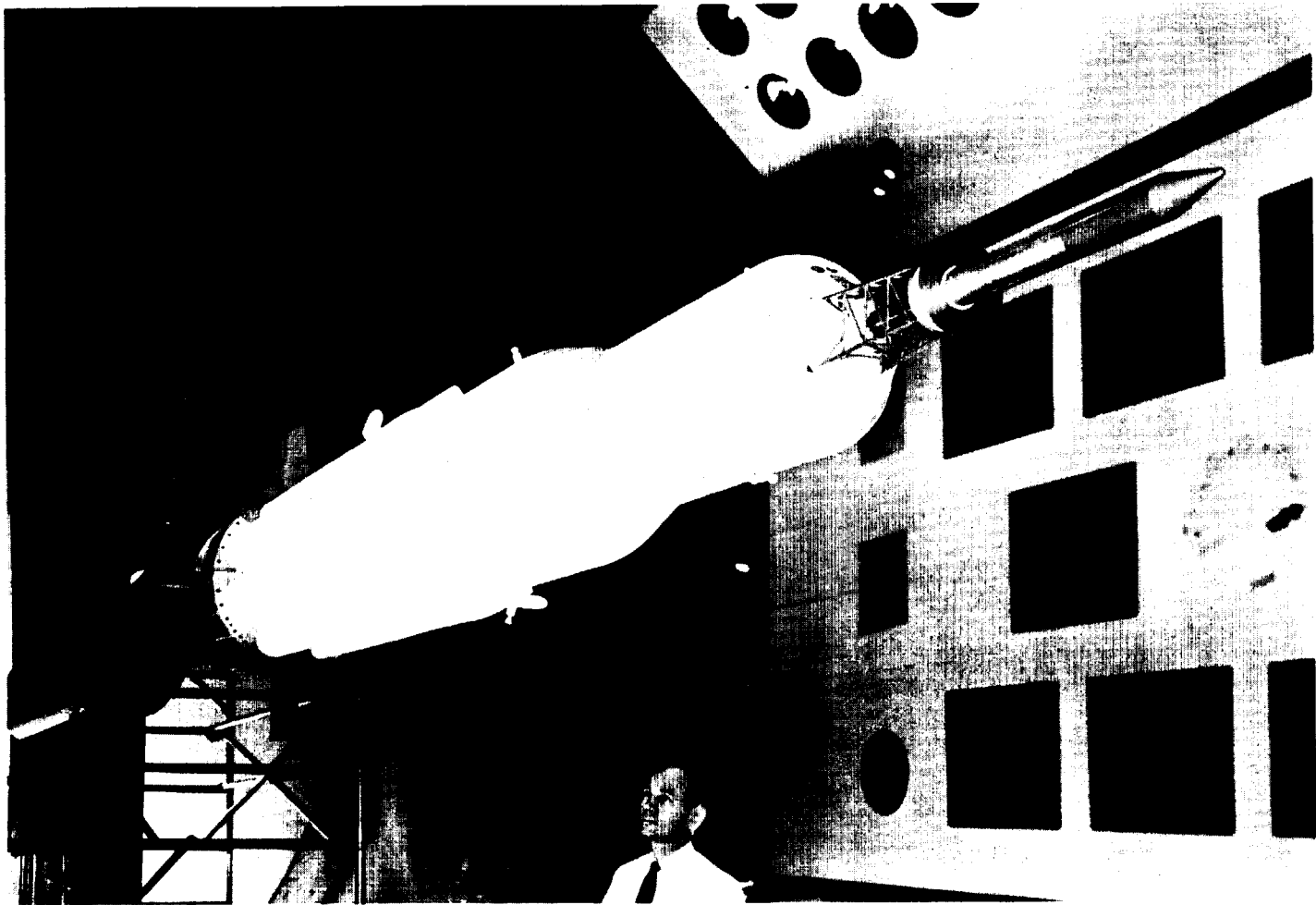
Figure 11.- Eight-percent aeroelastic buffet model mounted in tunnel.

NORMALIZED POWER
SPECTRAL DENSITY

SATURN-APOLLO MODEL
M=0.90

FREQUENCY, CPS
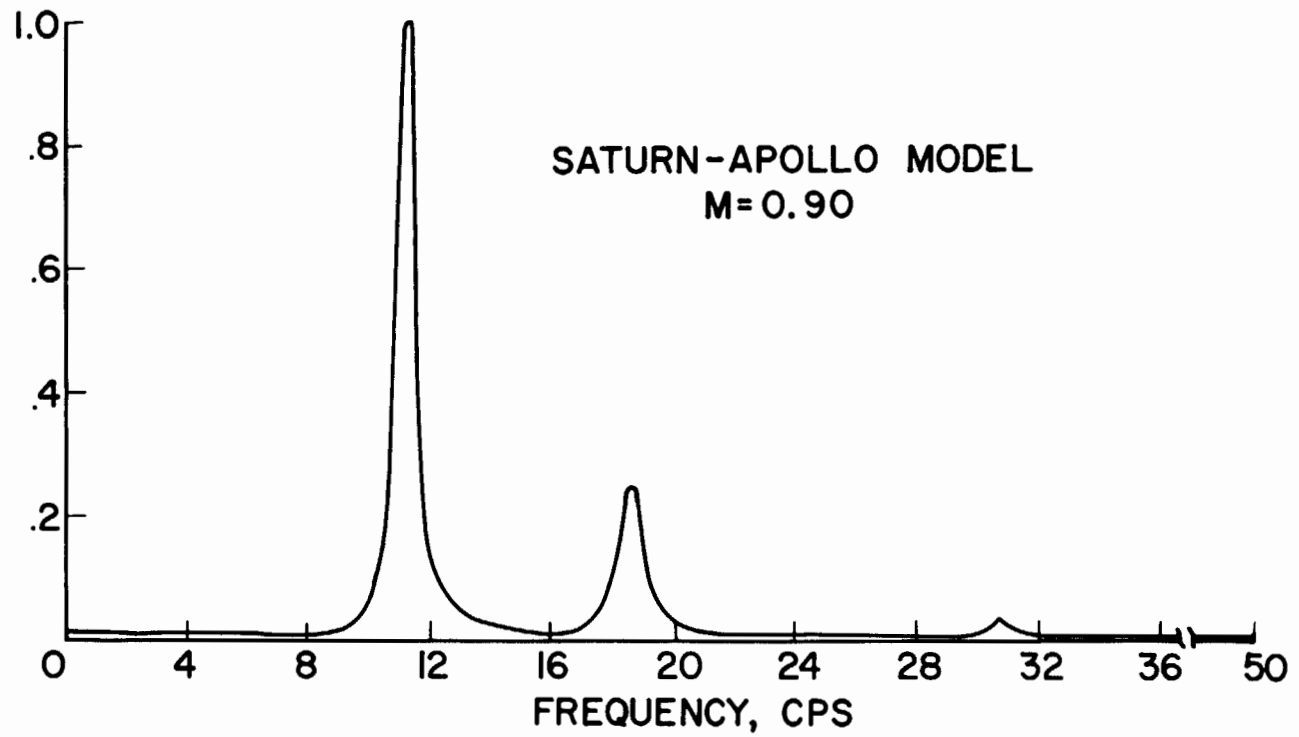
NASA

Figure 12.- Bending-moment power spectrum for Saturn-Apollo aeroelastic model at M = 0.90.

38
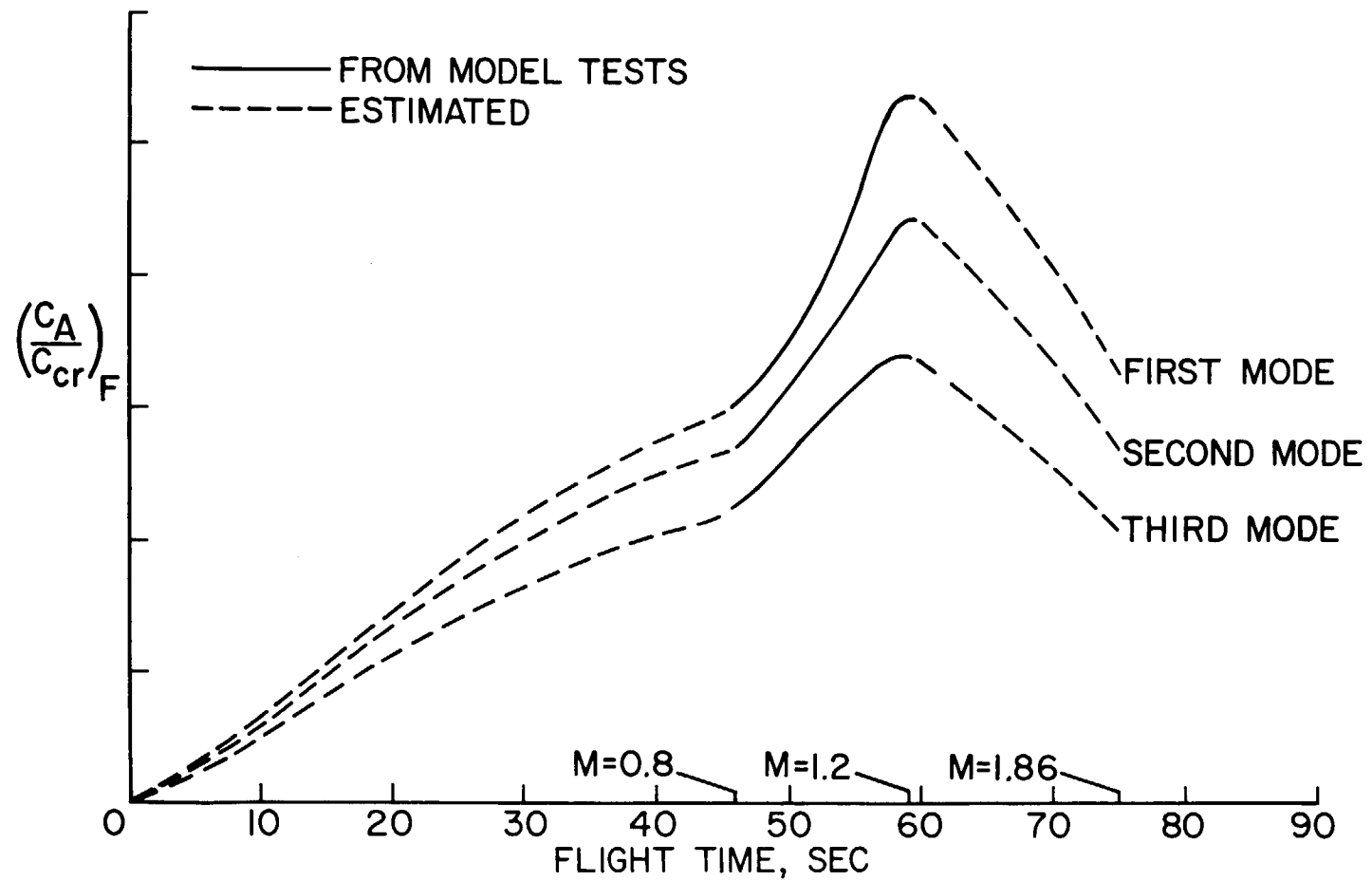
Figure 13.- Full-scale Saturn-Apollo aerodynamic damping predicted from model tests.

NASA

FULL-SCALE
BENDING
MOMENT

FIRST MODE
SECOND MODE
THIRD MODE

FULL-SCALE STATION, IN.
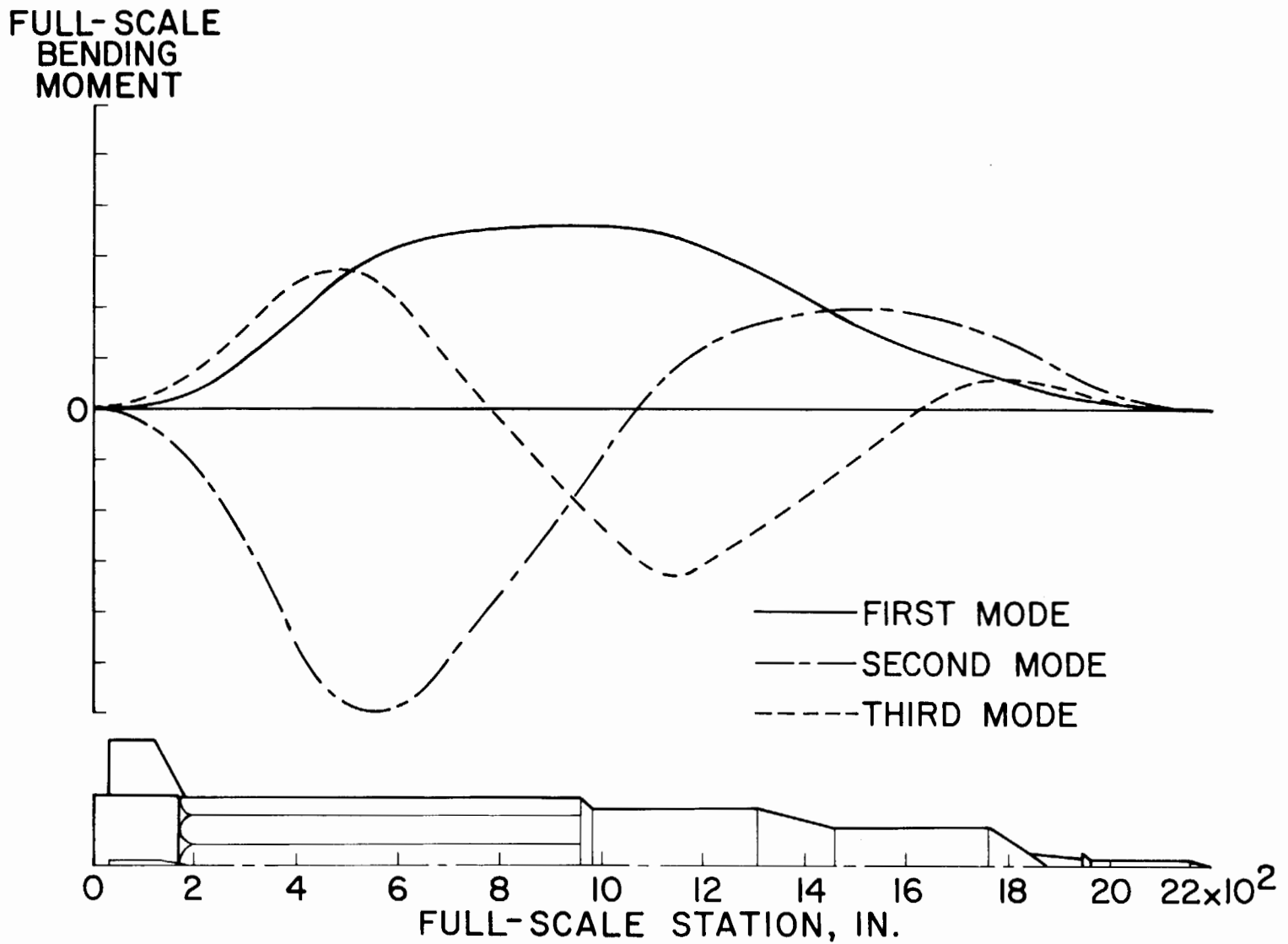
NASA

Figure 14.- Full-scale rms bending-moment distribution for first three bending modes
of Saturn-Apollo vehicle at M = 0.9 predicted from model tests.

40

FULL-SCALE
TOTAL
BENDING
MOMENT

——— 0° ANGLE OF ATTACK
- - - - 6° ANGLE OF ATTACK

FULL-SCALE STATION, IN.

$0 \quad 2 \quad 4 \quad 6 \quad 8 \quad 10 \quad 12 \quad 14 \quad 16 \quad 18 \quad 20 \quad 22 \times 10^2$
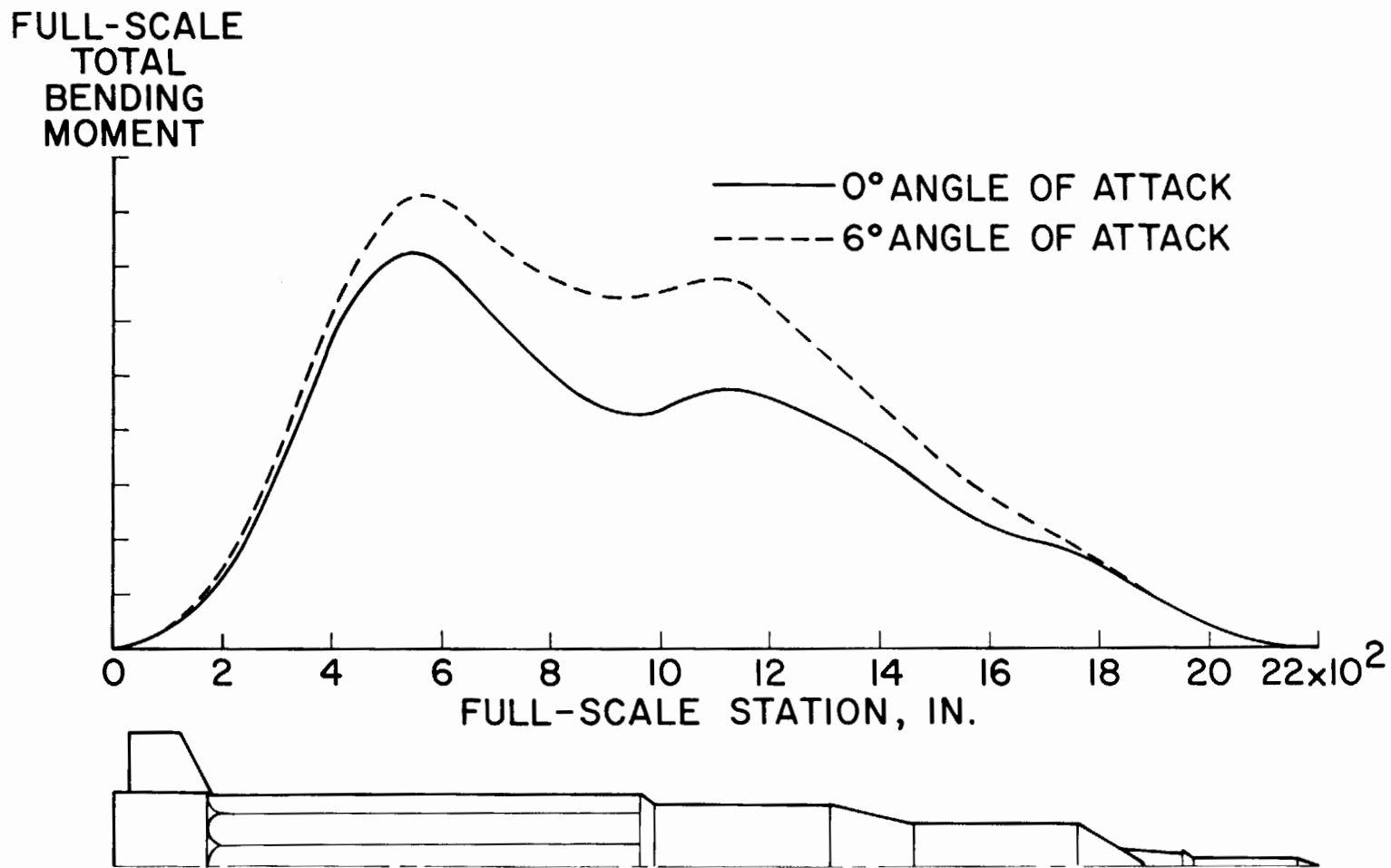
NASA

Figure 15.- Total full-scale rms buffet bending-moment distribution at M = 0.9 predicted from model tests.

41

OSCILLATING LIFT

STEADY LIFT

STEADY DRAG

OSCILLATING
DRAG

VORTEX
SHEDDING

STEADY
GROUND-WIND
PROFILE

ATMOSPHERIC
GUSTS AND
TURBULENCE
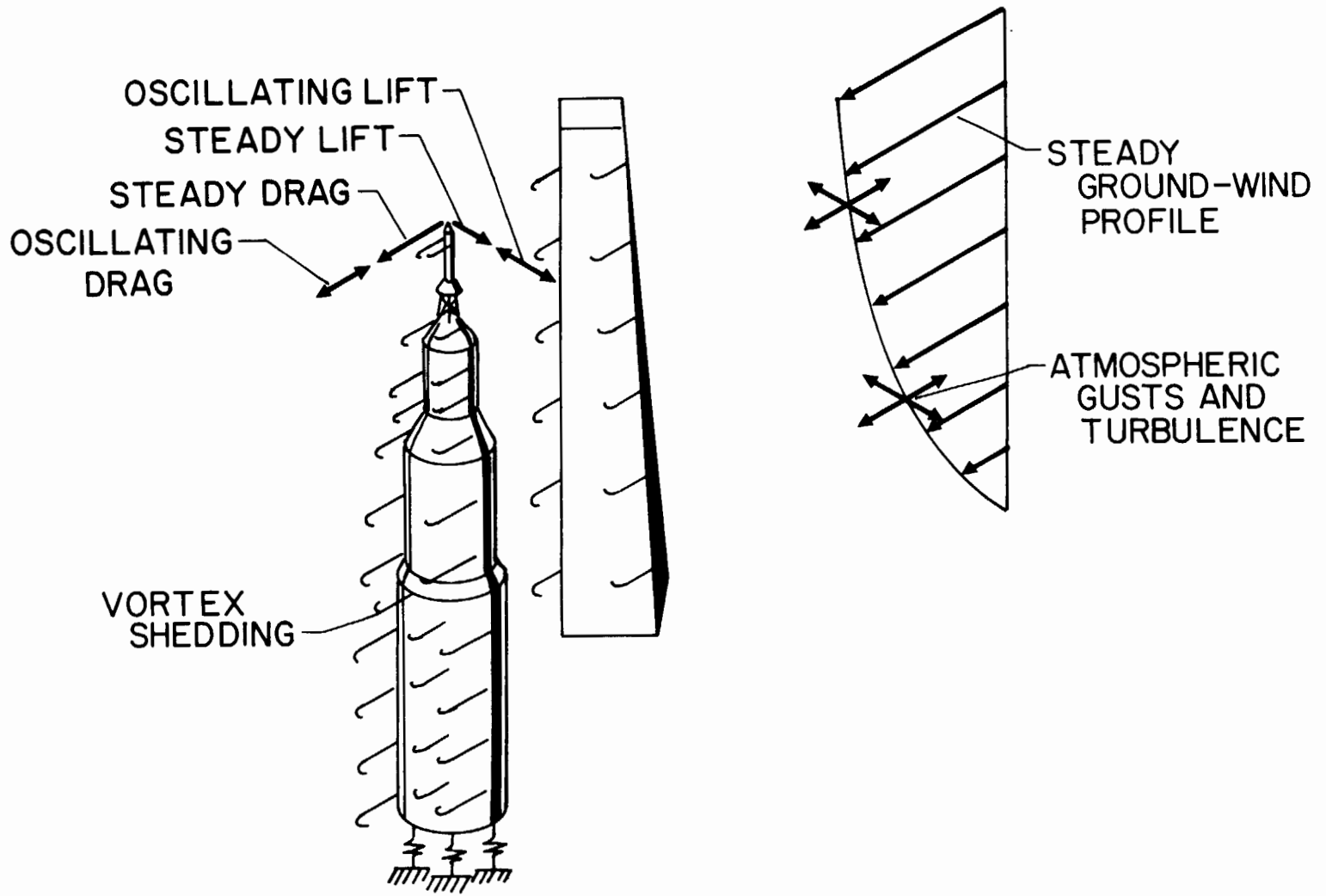
NASA

Figure 16.- Load conditions caused by ground winds.

42
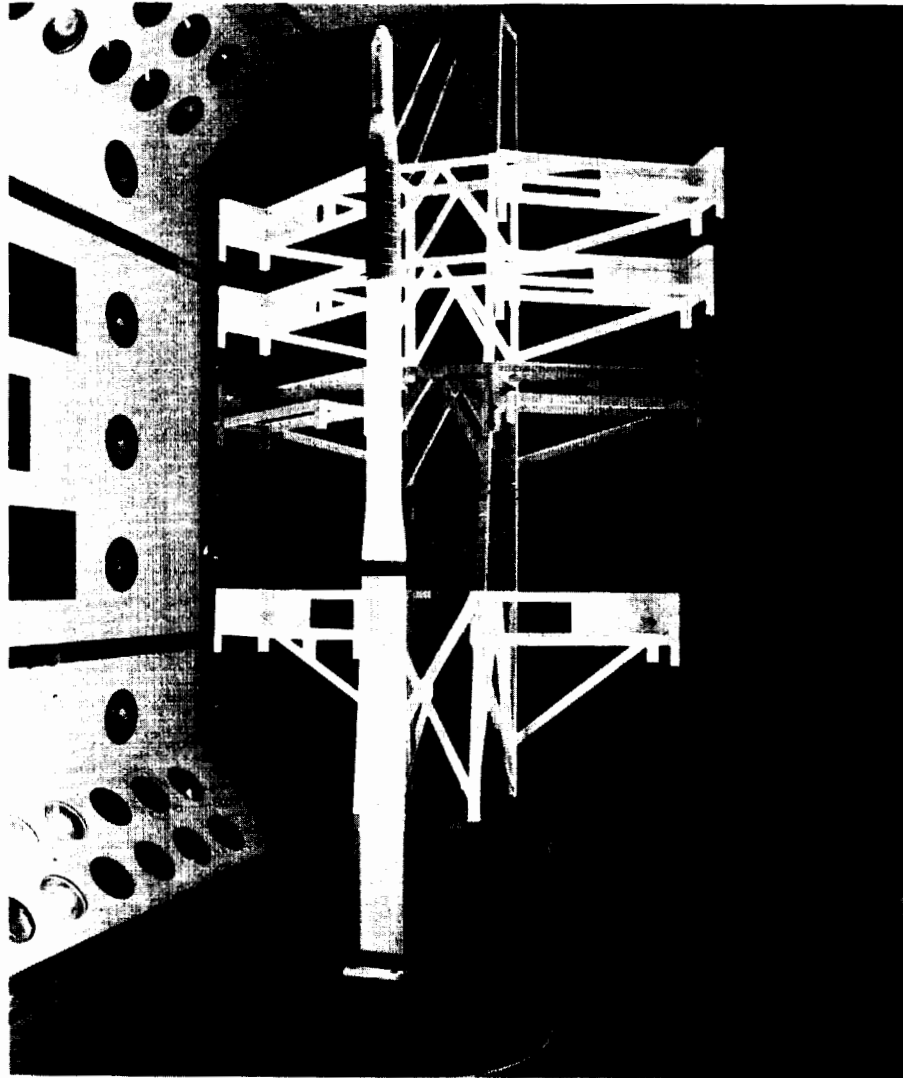
(a) 15-percent scale Scout ground-wind loads model.

NASA
L-60-6687

Figure 17.- Some ground wind models tested in Langley Research Center transonic dynamics tunnel.
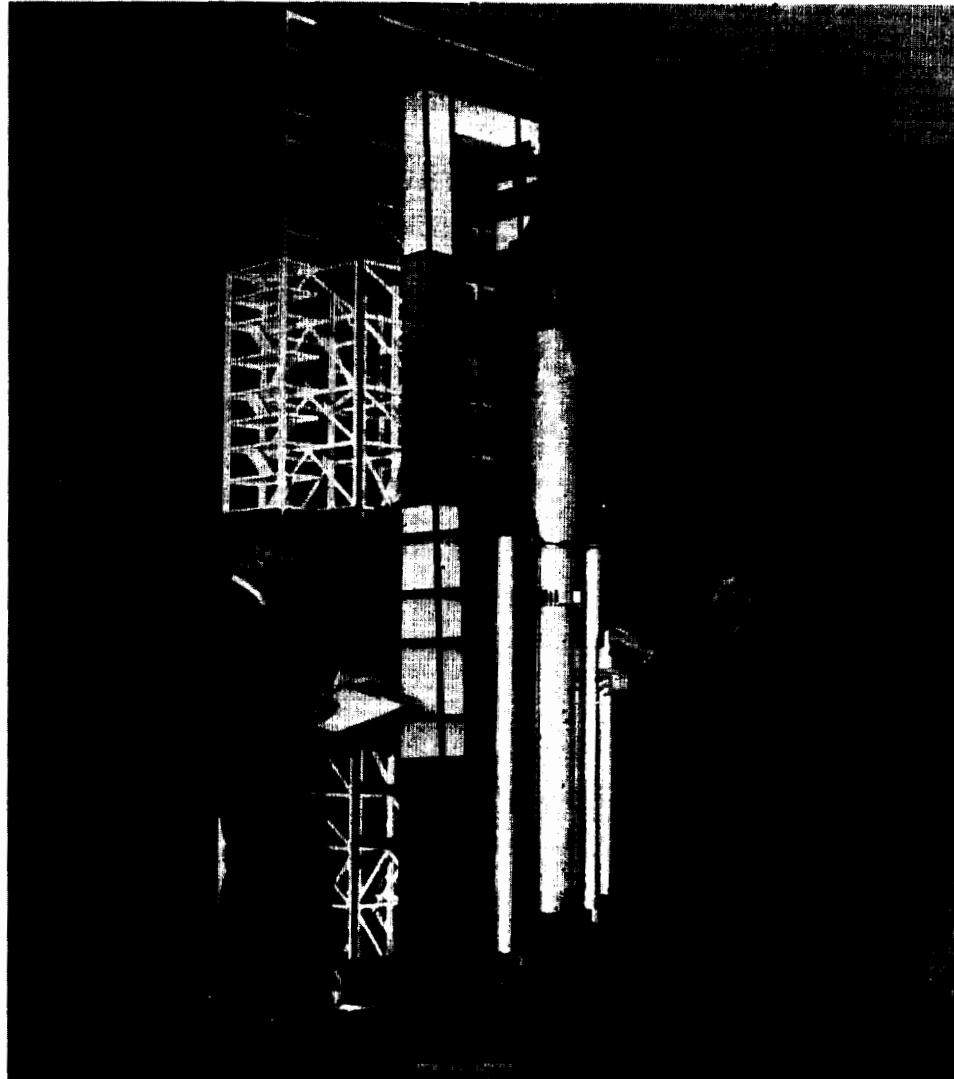
(b) 7.5-percent scale Titan III ground-wind loads model
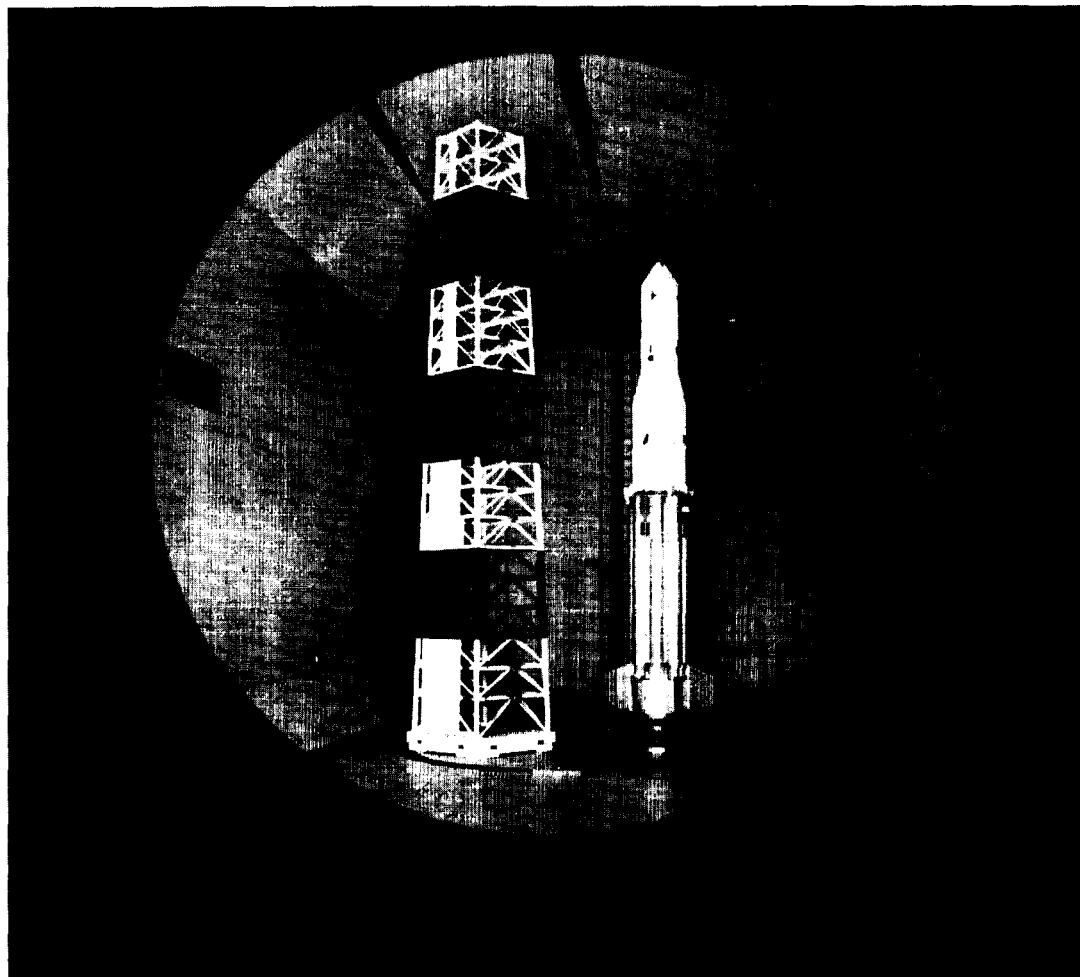with Dyna Soar payload.

NASA
L-63-312

Figure 17.- Continued.
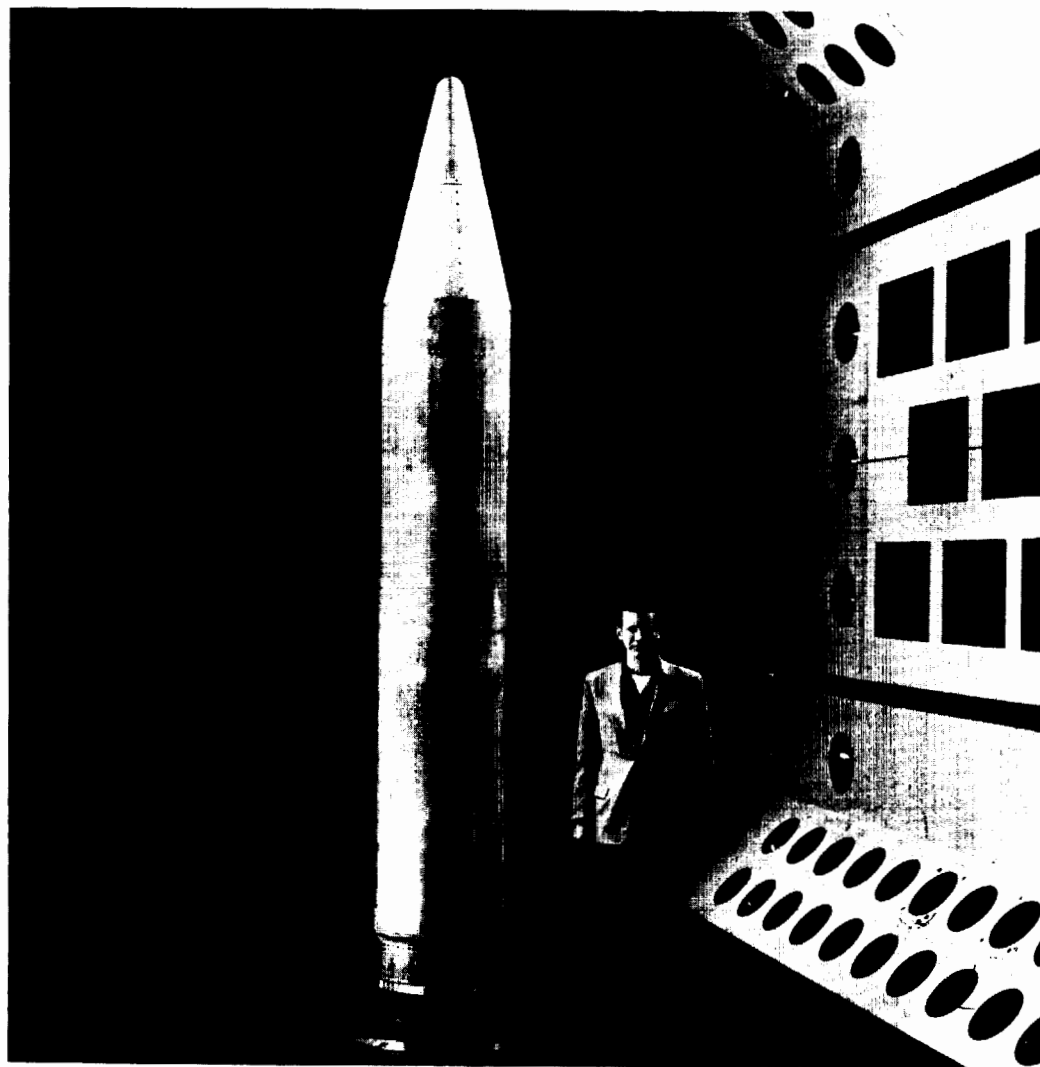
(c) 20-percent scale Jupiter ground-wind loads model.
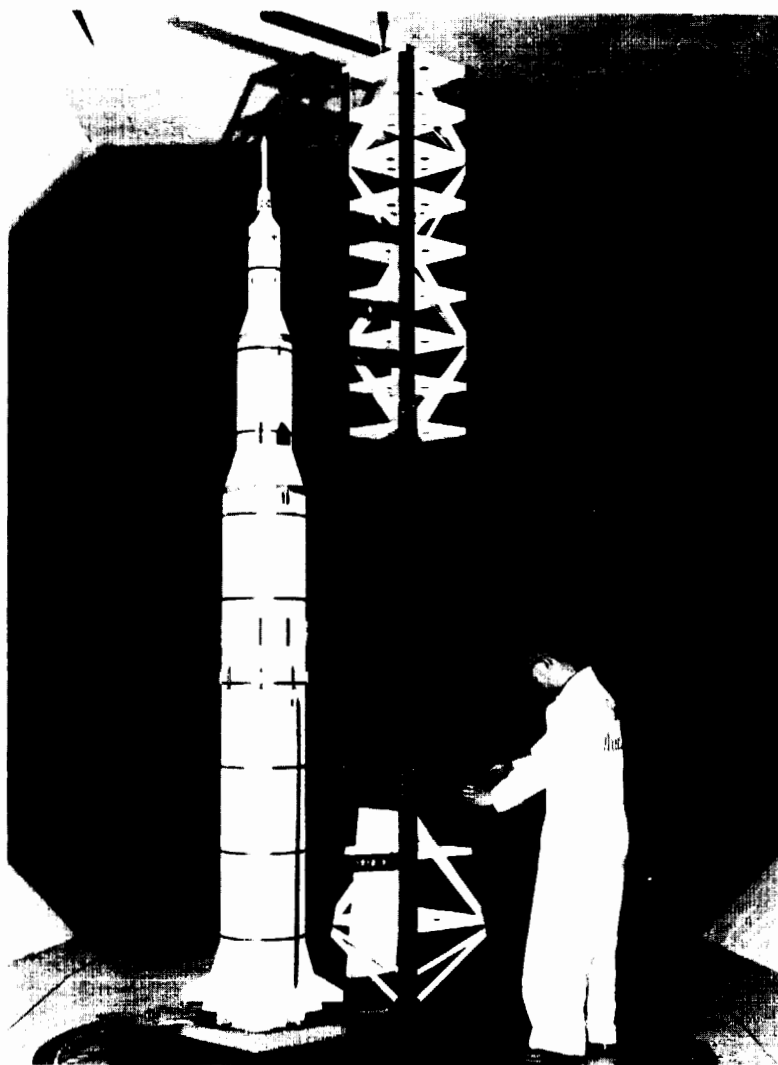
Figure 17.- Continued.

NASA
L-61-7179

(d) 7-percent scale Saturn 1-Block 11 ground-wind loads model.
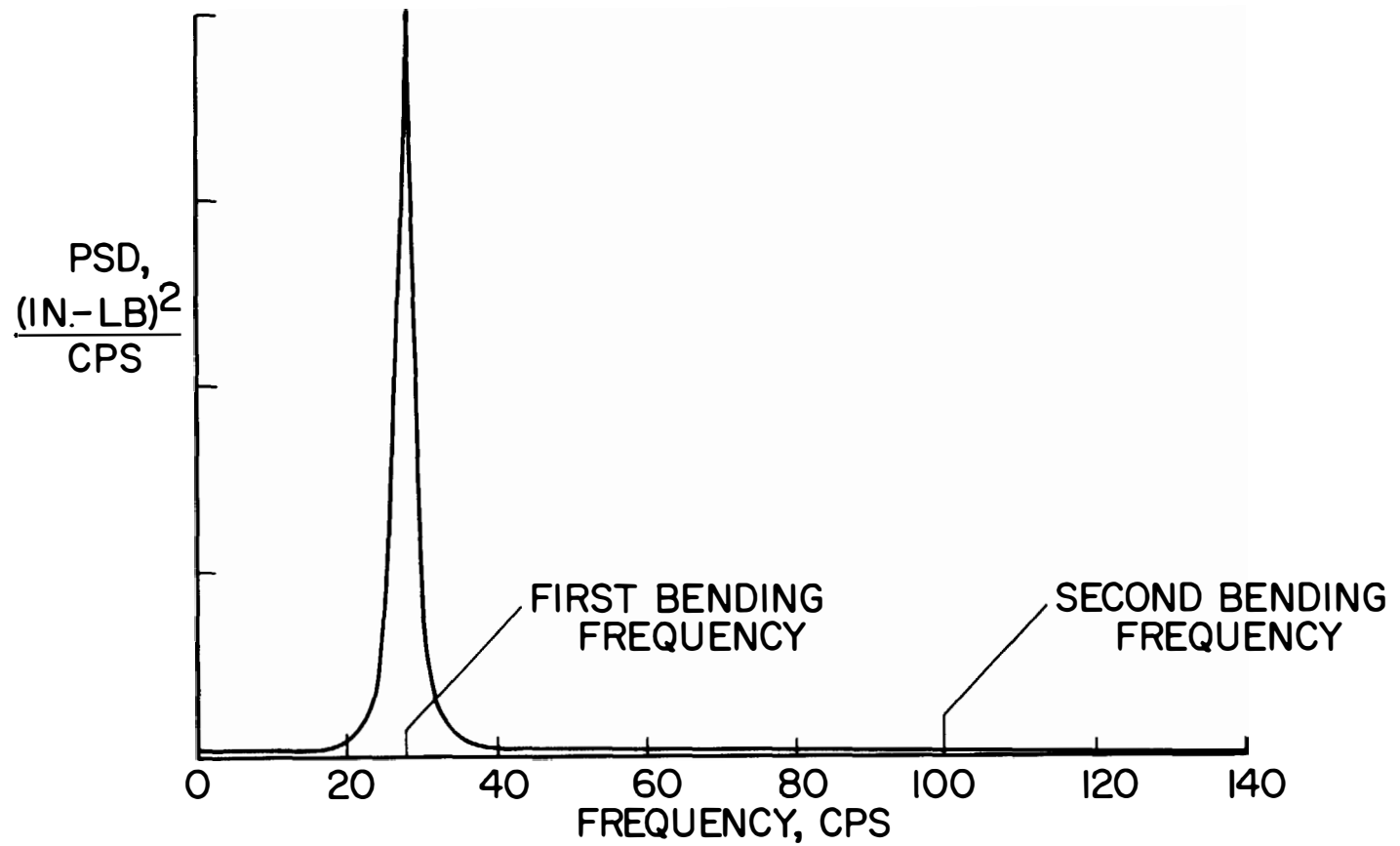
Figure 17.- Continued.

NASA
L-63-382

(e) 3-percent scale Saturn V ground-winds loads model.
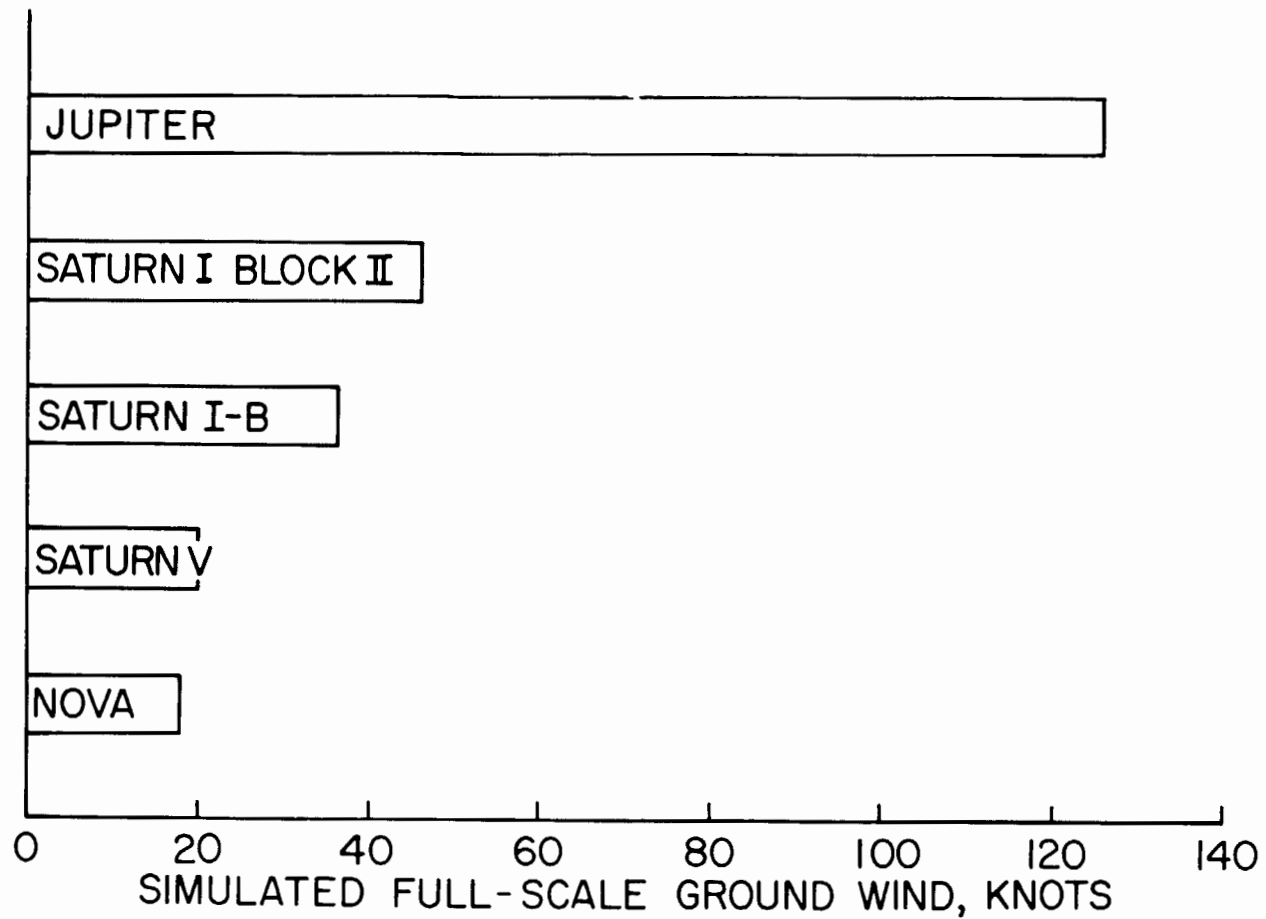
Figure 17.- Concluded.

NASA
L-63-2701

PSD,

$\dfrac{(\text{IN.-LB})^2}{\text{CPS}}$

FIRST BENDING
FREQUENCY

SECOND BENDING
FREQUENCY

0   20   40   60   80   100   120   140
FREQUENCY, CPS

Figure 18.- Typical power spectral density of base bending-moment response of
launch vehicle ground winds model.

$$R_{N,M} = R_{N,F} \text{ AND } M = 0.4$$

Figure 19.- Velocity simulation range available for ground-wind launch vehicle models in Langley Research Center 16-foot transonic dynamics tunnel.
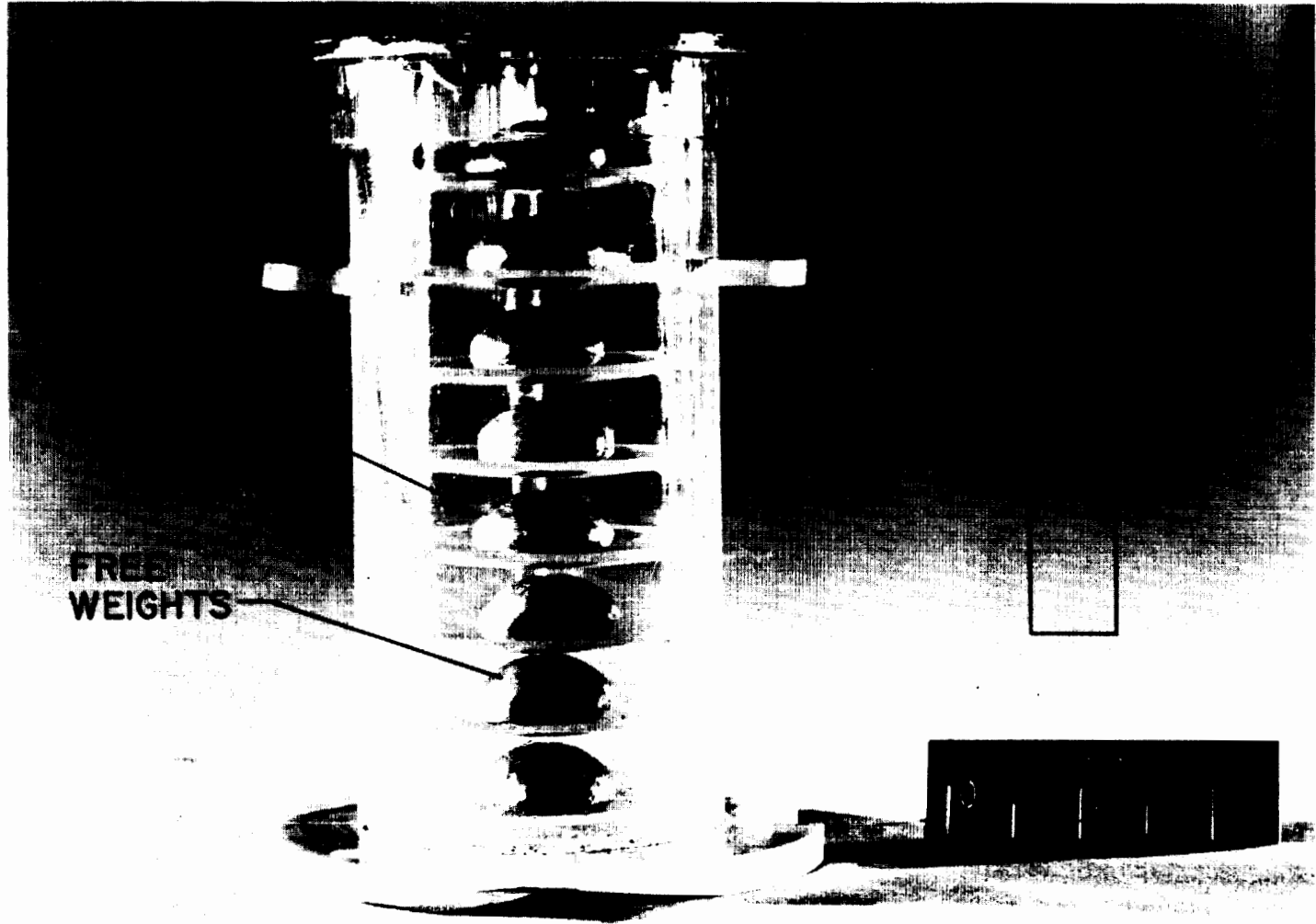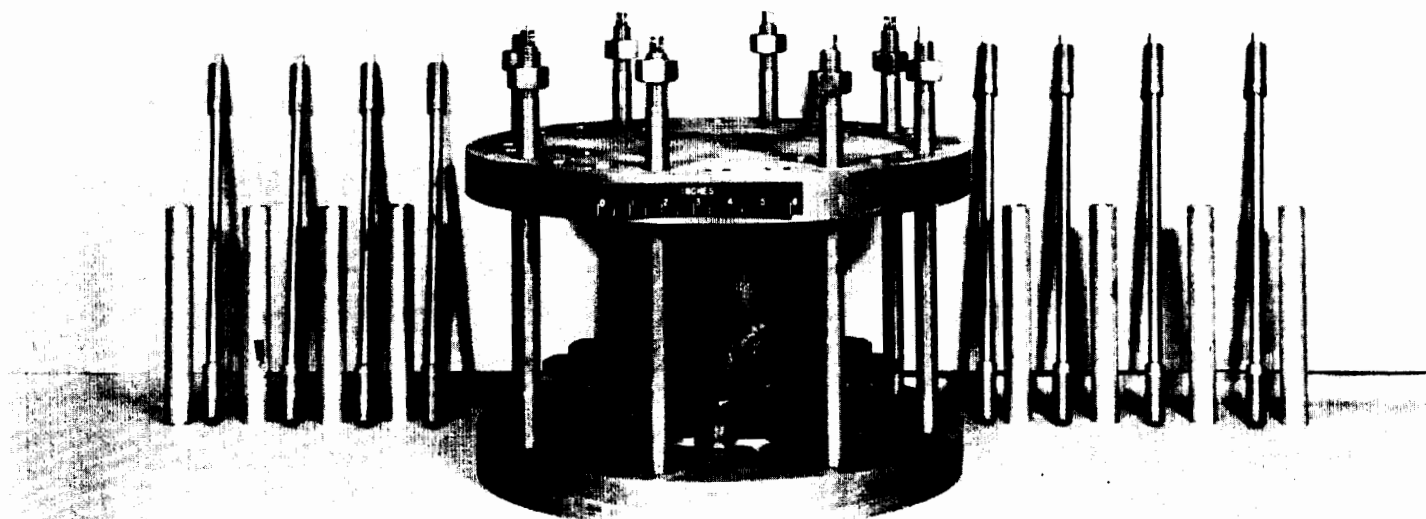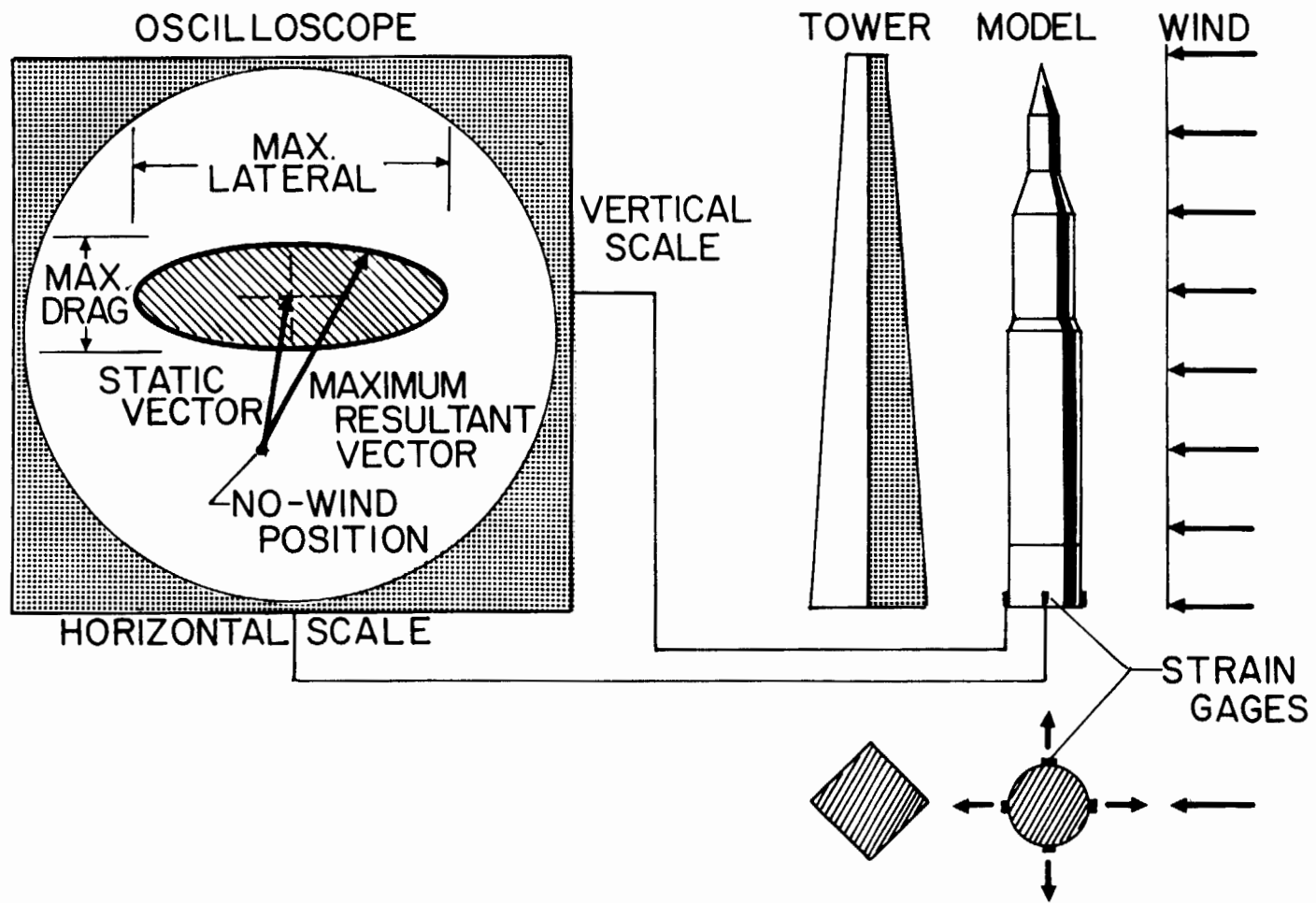
NASA

FREE
WEIGHTS

NASA
L-63-5491

Figure 20.- Model variable structural damper.

50

Figure 21.- Photograph of variable stiffness base mounting fixture.

OSCILLOSCOPE   TOWER   MODEL   WIND
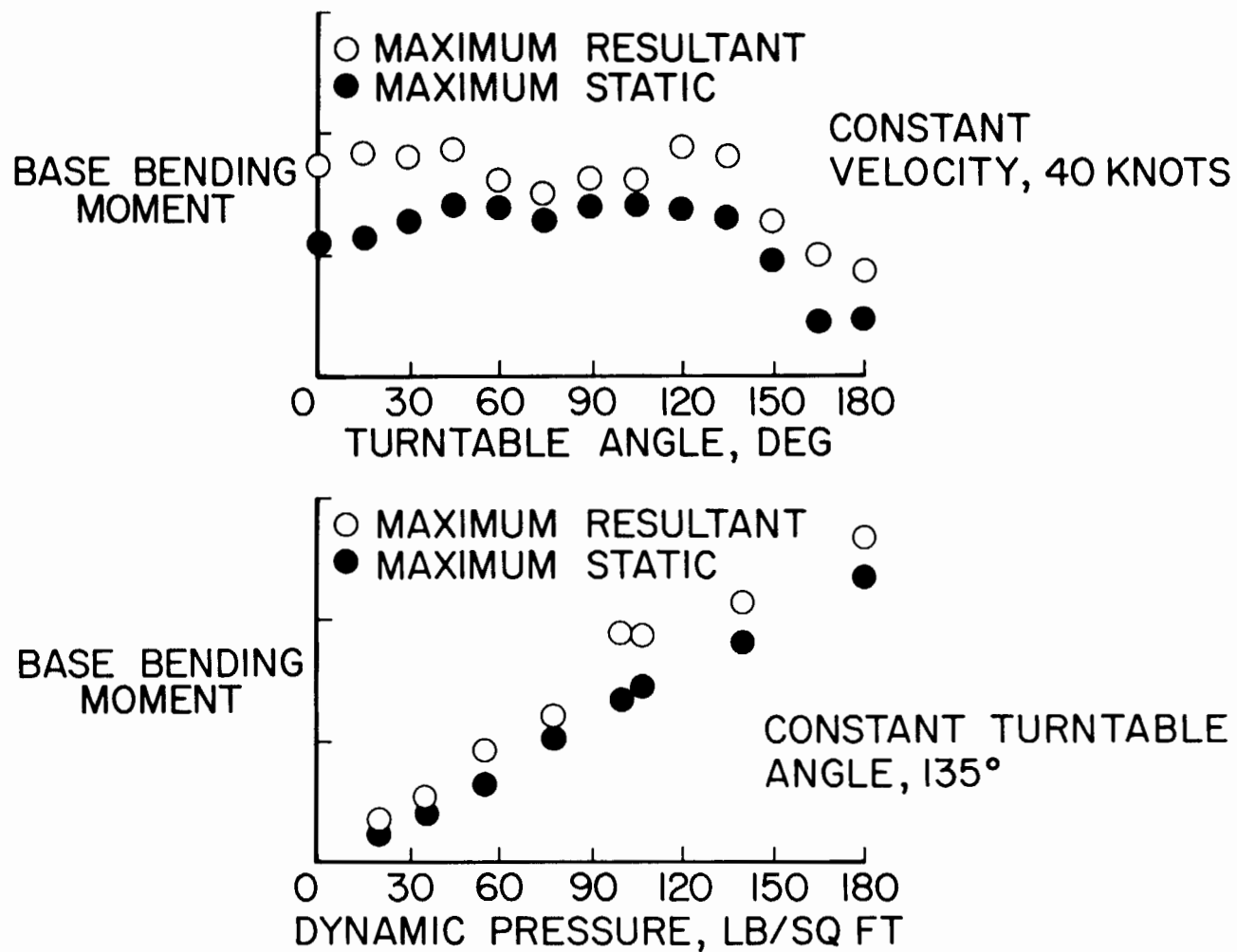
MAX. LATERAL

MAX. DRAG

VERTICAL SCALE

STATIC VECTOR

MAXIMUM RESULTANT VECTOR

NO-WIND POSITION

HORIZONTAL SCALE

STRAIN GAGES

NASA

Figure 22.- Schematic of oscilloscope time history of base bending-moment response.

SIMULATED 40 KNOT WIND FROM VARIOUS AZIMUTH ANGLES

LAUNCH VEHICLE MODEL

UMBILICAL TOWER

STEADY BENDING MOMENT

MAX. RESULTANT BENDING MOMENT

0°
45°
90°
135°
180°
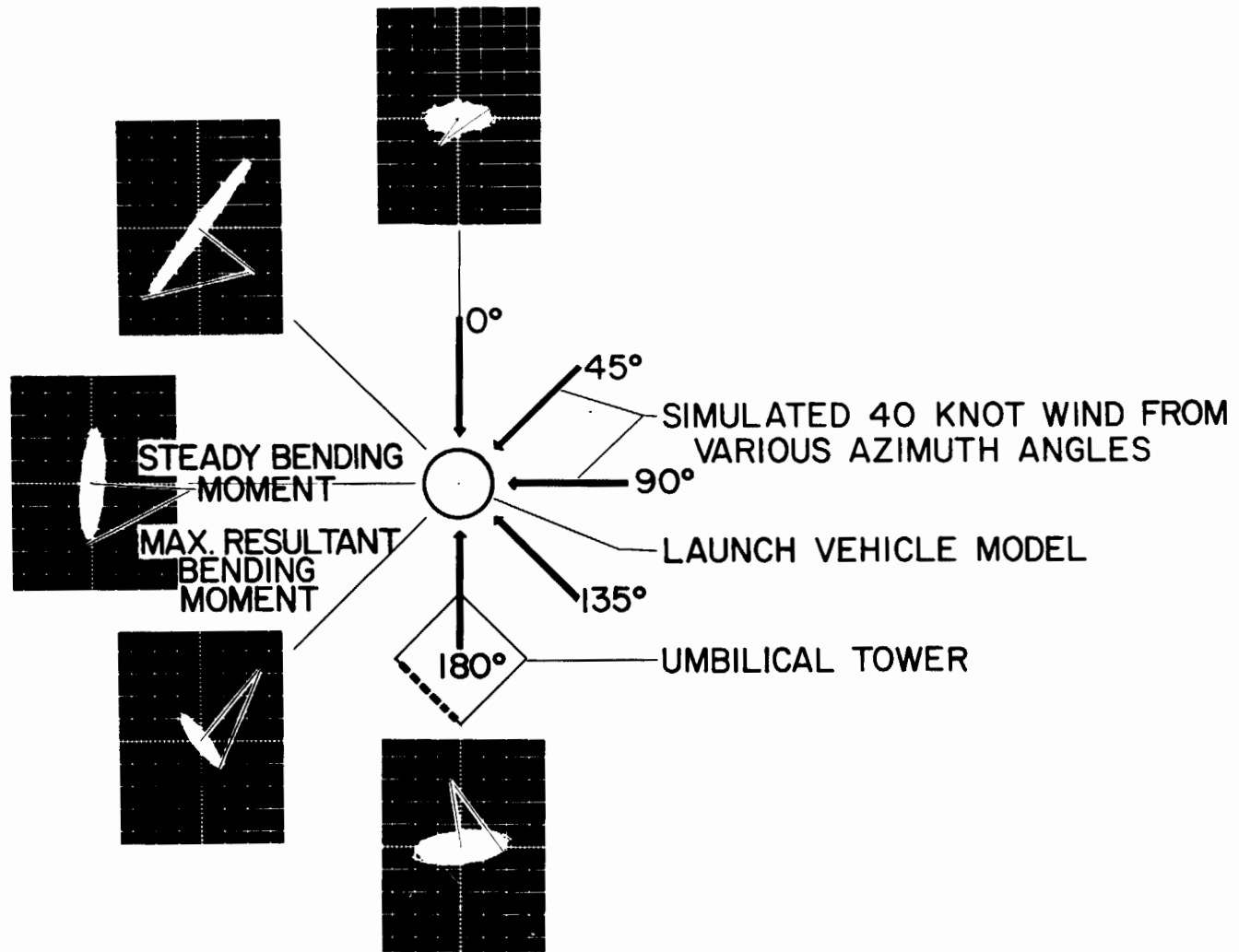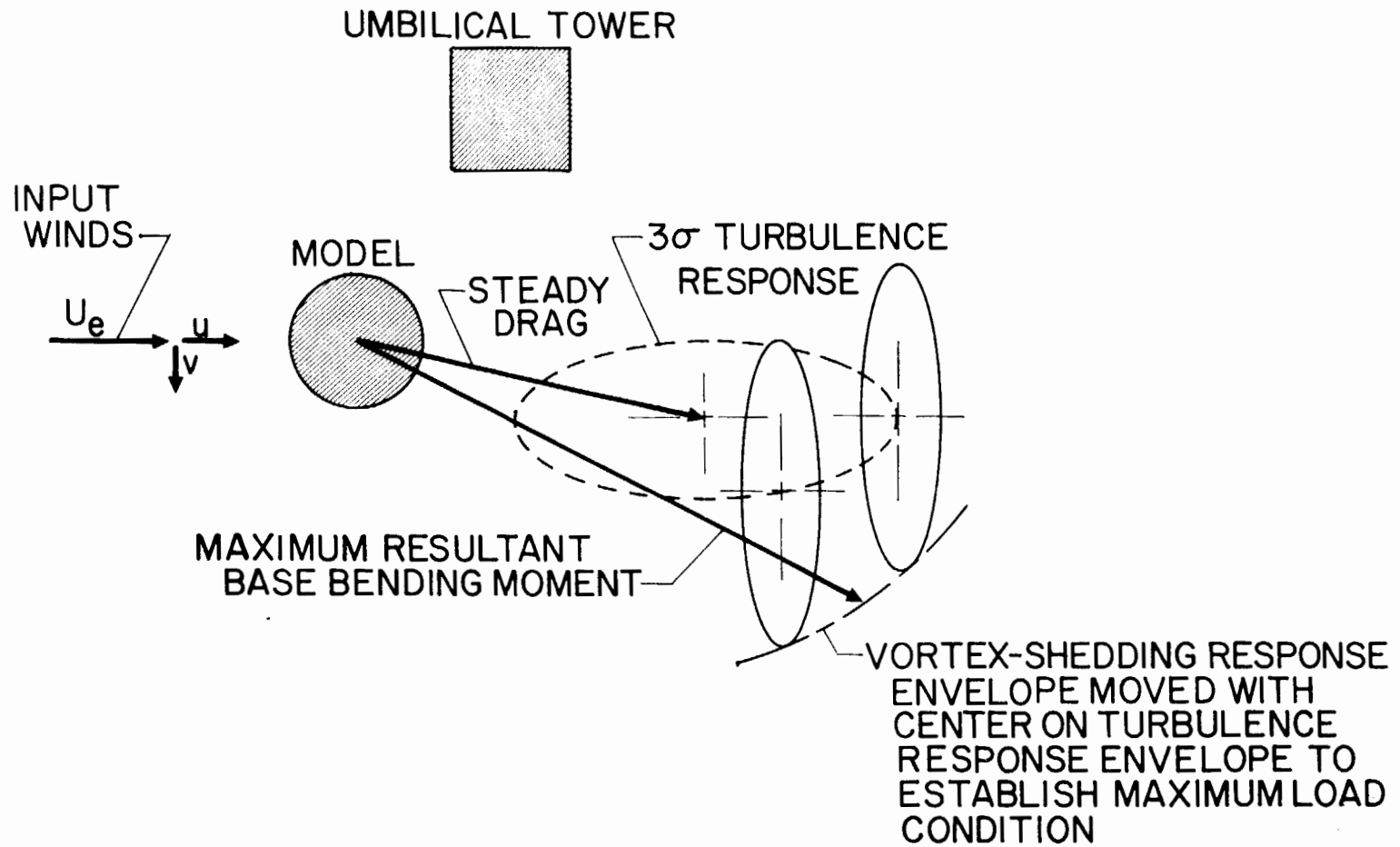
NASA

Figure 23.- Illustration of bending-moment response to winds from various azimuth angles.

○ MAXIMUM RESULTANT
● MAXIMUM STATIC

CONSTANT
VELOCITY, 40 KNOTS

BASE BENDING
MOMENT

O   30   60   90   120 150 180
TURNTABLE ANGLE, DEG

○ MAXIMUM RESULTANT
● MAXIMUM STATIC

BASE BENDING
MOMENT

CONSTANT TURNTABLE
ANGLE, 135°

O   30   60   90   120 150 180
DYNAMIC PRESSURE, LB/SQ FT

NASA

Figure 24.- Variation of maximum static and total base bending moment with turntable angle
and dynamic pressure.

Figure 25.- Method of combining wind tunnel and theoretical ground wind loads.